Numerical Analysis of Dielectrophoretic Bio-Separation Using Slanted Electrodes

by Bahar Kazemi, Bachelor of Science

A Thesis Submitted in Partial
Fulfillment of the Requirements
for the Degree of
Master of Science
in the field of Mechanical Engineering

Advisory Committee:

Jeff Darabi, Chair

Majid Molki

Mohammad Shavezipour

Graduate School
Southern Illinois University Edwardsville
December, 2017

ABSTRACT

NUMERICAL ANALYSIS OF DIELECTROPHORETIC BIO-SEPARATION USING SLANTED ELECTRODES

by

BAHAR KAZEMI

Chairperson: Professor Jeff Darabi

This study presents the numerical simulation and optimization of a dielectrophoretic bio-separation chip for isolating bioparticles such as circulating tumor cells (CTCs), or different strands of E.coli bacteria. The chip consists of ten pairs of electrodes placed with an angle of 10° with respect to the direction of the flow on the top and bottom walls of the channel. The spatially non-uniform electric field produced by the slanted electrodes applies a repulsive force on the particles that are flowing through the channel. The repulsive force applied by the top and bottom electrodes are balanced and the particles stay at the centerline throughout the channel. On the other hand, the magnitude of forces resulted from electric field in the x and z-directions deflects particles depending on their size and guides them towards different outlets. Numerical simulation of the particle-fluid transport was performed using an open-source software named OpenFOAM and the deflection of the particles within the microfluidic channel was predicted. The present computational domain considers the dominant forces such as dielectrophoretic and hydrodynamic forces as well as their effects on the design and operating parameters of the chip. The results show that this device is capable of separating various cells of different sizes from their native environment. Furthermore, a parametric study was performed to investigate the effect of voltage, flow rate, number of electrodes, cell size, and channel height on the separation process and to improve the performance of the device.

ACKNOWLEDGEMENTS

I would like to thank Dr. Jeff Darabi who, as my teacher and mentor, has taught me more than I could ever give him credit for here. He has supported me continuously with his patience and immense knowledge throughout this research, and has shown me, by his example, what a good researcher should be. I would like to extend a thank you to Dr. Majid Molki who introduced OpenFOAM to me and smoothed the path for me to perform this research. I would also like to acknowledge Dr. Mohammad Shavezipour for serving as my committee member even at hardship, and thank you for letting my defense be an enjoyable moment. I would like to thank my dear friend, Matin Golozar, who helped me with learning the software and who continuously supported me with his feed-backs and comments on this research. I truly appreciate everything he has done for me.

Nobody has been more important to me in the pursuit of this project than the members of my family. I would like to thank my father for his unfailing support and continuous encouragement throughout my study. I would also like to thank my mother, whose love and guidance are with me in whatever I pursue. My parents are the ultimate role models. I would also like to thank my little brother for his love and unwavering belief in me. This accomplishment would not have been possible without you.

Author

Bahar Kazemi

TABLE OF CONTENTS

LIST OF FIGURES

LIST OF TABLES

NOMENCLATURE

Abbreviations

DEP	Dielectrophoresis
AC	Alternating Current
DC	Direct Current
$DC-iDEP$	direct current insulator-based dielectrophoresi
$pDEP$	Positive Dielectrophoresis
$nDEP$	Negative Dielectrophoresis
$MACS$	Magnetic-Activated Cell Sorter
$FACS$	Fluorescence-Activated Cell Sorter
CFD	Computational Fluid Dynamics
LOC	Lab-On-a-Chip
rms	Root Mean Squared
$OpenFOAM$	Open Field Operation and Manipulation
FV	Finite Volume
FV	Control Volume
N	north
S	south
W	west
E	east
NW	northwest
NE	northeast
SW	southwest
SE	southeast
$SIMPLE$	Semi-Implicit Method for Pressure-Linked Equations
$GAMG$	Geometric-Algebraic Multi-Grid
PCG	Preconditioned Conjugate Gradien
CPU	Central Processing Unit

Greek Letter

ϵ_m	permittivity of the medium
μ	fluid dynamic viscosity
ρ_E	net free charge density
ϕ	electrical potential
ϵ	permittivity
ϵ_p	permittivity of the particle
ϵ^*	complex permittivity
ω	angular frequenc
Γ_ϕ	diffusivity of the quantity ϕ
ν	fluid kinematic viscosity
Ω	volume
τ_{ij}	stress tensor

Latin Characters

A	face area
$\vec{E}$	electric field vector
D	electric displacement, electric flux density
t	time
u	velocity
p	pressure, point in the center of the control volume
Re	Reynolds number
u^*	normalized velocity
t^*	normalized time
p^*	normalized pressure
m_p	mass of the particle
u_p	particle velocity
F_{DEP}	dielectrophoretic force
F_d	drag force
F_g	gravitational force
F_B	brownian motion
a	radius
f_{CM}	Clausius-Mossotti factor
i, j, k	unit vectors
V_{p-p}	peak-to-peak voltage
V_{rms}	rms voltage
u_f	fluid velocity
g	gravitational constant
x	displacement
D	diffusivity

K_B	Boltzmann's constant
T	temperature
d_p	diameter of the particle
$\|F\|$	magnitude of force
n	normal vector
x, y, z	components of Cartesian coordinates
$u_{i,j}$	velocity component in i and j directions
$\vec{x_p}$	position of the center of the particle
L	liter
h	hour
F_x	x-component of the force
F_y	y-component of the force
F_z	z-component of the force
V	voltage
s	second

CHAPTER 1

INTRODUCTION

1.1 Dielectrophoresis

Separating bioparticles from complex mixtures and screening them is of great importance in many diagnostic and therapeutic applications. With the advent of lab-on-a-chip (LOC) devices, the process of screening and handling these particles has become less challenging than before. There are numerous methods used in lab-on-a-chip devices to perform the process of sorting or separation of bioparticles. Dielectrophoresis (DEP) is a term applied to the motion of particles in a non-uniform, alternating electric field [1]. Due to the non-uniformity of the field, there is no need for the particles to be electrically charged [2]. In fact, the movement of the particles is due to polarization which is resulted from a dipole moment produced by the non-uniformities of the electric field. The polarization accumulates the positive and negative charges on the opposite sides of the particle. As it is illustrated in Figure 1.1, if the electric field is uniform, the Columbic forces on the opposite sides of the particle cancel each other and the particle does not move. On the other hand, if the electric field is non-uniform, the Columbic forces are not equal and the particle begins moving in the medium [3].

One of the parameters that the dielectrophoretic force depends on is the volume of the particle. That is why dielectrophoresis is used as a tool to separate bioparticles of different sizes and to lead them through different collecting outlets [4]. non-uniformities can be generated using either DC or AC electric fields. A neutral particle can be polarized under the influence of a DC electric field. The positive nuclei of the particle is attracted towards the negative electrode and the negative electrons are attracted by the positive electrode. If the field is uniform, the forces on the particle are equal but opposite in direction and there will be no translational motion. However, if the field is not uniform,

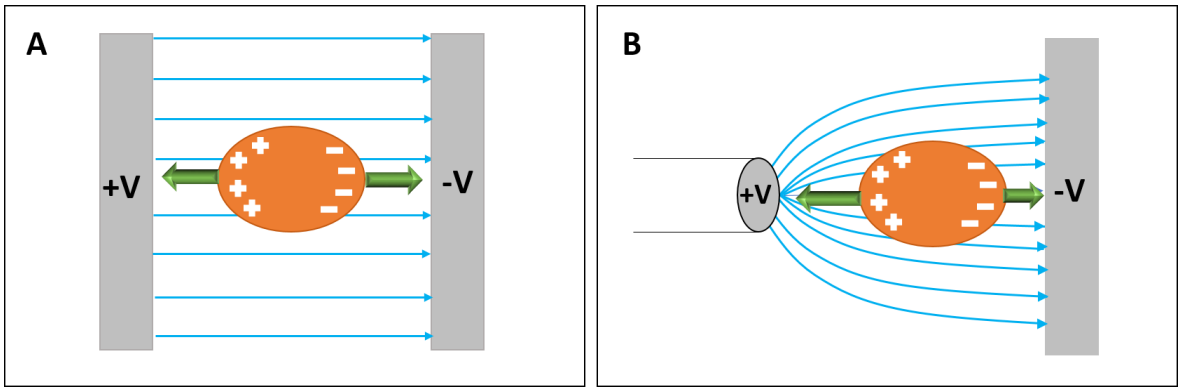

Figure 1.1: Particle polarization in: A) a uniform electric field, and B) a non-uniform electric field

the forces do not balance and the particle begins to move towards one of the electrodes [5]. One way to generate non-uniformities in a DC electric field is using embedded obstacles which are electrically insulated. These obstacles could be hurdles, steps or other features embedded in the microfluidic channel [6]. This method is called direct current insulator-based dielectrophoresis (DC-iDEP) [7]. In DC-iDEP electrodes are located at the end of the channels [8]. non-uniformities can also occurs in an AC electric field. In an AC field, polarizability of the particles depends on the frequency along with the value of the voltage, and the phase. The frequency dependency of the particle is defined in this way that a value of frequency might affect the motion of one type of particle but not the others. Phase also creates non-uniform electric fields which result in traveling waves. There is a phase-shift between each of the two electrodes when they are arranged in a way that each of them reaches their peak voltage at a different time from the others [5]. In general, in most DEP applications, AC electric fields are used. There are two types of dielectrophoresis. If the permeability of the particle is greater than that of the surrounding medium, the particle moves towards the regions in which the electric field is stronger. This phenomenon is called positive dielectrophoresis (pDEP). In contrast, negative dielectrophoresis (nDEP) occurs when the permeability of the particle is less than that of the medium and the particle is repelled from the regions with higher electric

field and moves towards regions with lower field gradients. [4]. The advantage of using nDEP instead of pDEP is that because there is no contact between the particles and the electrodes, less stress and less damage is exerted on the particles. Therefore, the viability of the particles are maintained [9].

1.2 The Superiority of Using Microelectrodes

In the very first applications of dielectrophoresis, electrode dimensions were in the scale of millimeter; much larger than the size of the particles [10]. These electrodes needed high voltages to operate and produced high temperatures which resulted in heating effects. With the advent of microfabrication technologies and the ability to produce microelectrodes, dielectrophoresis turned into a practical method which could be utilized in lab-on-a-chip devices. One of the parameters that the dielectrophoretic force depends on is ∇E^2. The unit of ∇E^2 is V^2/m^3. By reducing the size of the electrodes, a lower voltage is needed to produce an electric field with the same strength. For instance, if the dimensions of the electrode are reduced by a factor of n, then the voltage must be reduced by a factor of $(n)^{3/2}$ to produce an electric field with the same strength. Therefore, one of the advantages of using microelectrodes is lower values of operating voltage. Additionally, using microelectrodes result in lower heating and electrochemical effects. Since, in general, microelectrodes produce weaker electric fields and the electrical heating effects are lower in contrast to electrodes with larger scales [11]. In addition, microelectrodes have smaller surface areas in contact with the surrounding medium. As a result, the effects of electrochemical processes resulted from these contacts are less than that of electrodes with larger scales [12].

1.3 The Pros and Cons of DEP

Cell sorting and separating methodologies are of great importance in biomedical and pharmaceutical fields. There are three parameters with which the performance and

efficiency of a cell separation device is measured. Throughput measures the number of cell characterizations and sorting operations that are performed in a unit of time, purity is the ratio of target cells to non-target ones in the collection channel, recovery is the ratio of the target cells that are successfully separated in the collection channel to the total number of input cells. Among various methodologies, magnetic-activated cell sorters (MACS) and fluorescence-activated cell sorters (FACS) are the most common ones [13]. There are, however, some limitations in these two methods that DEP compensates for. FACS, for example, due to the serial screening of each cell, offers a high purity and recovery [14]. However, compared with MACS and DEP, the throughput is not high enough. On the other hand, MACS offers a high throughput due to its selection nature; but in contrast to conventional methods, the recovery and purity that this method offers is low [15]. Another significant advantage of DEP is that there is no need for labeling the cells with dielectrophoretic tags because bio-particles such as cells and DNA have dielectric properties and when an AC electric field is applied, large dipole moments are induced to the cells. Label-free methods impose less damage to the cell surface morphology which is why they are superior in biological applications [11]. Additionally, negative DEP is preferred to positive DEP because the particles are repelled from the electrodes and there is no contact between the electrodes and the particles. Thus, less damage is exerted on the particles and the viability and morphology of the cells are less affected [16]. There are also disadvantages associating with DEP. The fabrication of micro electrodes is a costly process compared with the fabrication of magnets in MACS. In addition, there are limitations on the applied voltage. If the voltage is too high, it could affect the cell viability and damage the cell internal structure. Furthermore, in very high voltages, electrolysis of the surrounding fluid may also occur [17].

1.4 The Scope of Research

A numerical simulation has been performed to model the translational migration of bioparticles in a non-uniform electric field. The particle-fluid motion and the electric field were simulated using an open-source software called OpenFOAM. The solver used to simulate separation is based on an Eulerian-Lagrangian CFD method that considers all the dominant forces acting on the particles. A parametric analysis was done to investigate the effect of particle size, voltage, flow rate, and the channel height. Furthermore, the numerical simulation was verified through several experimental publications performed by other research groups.

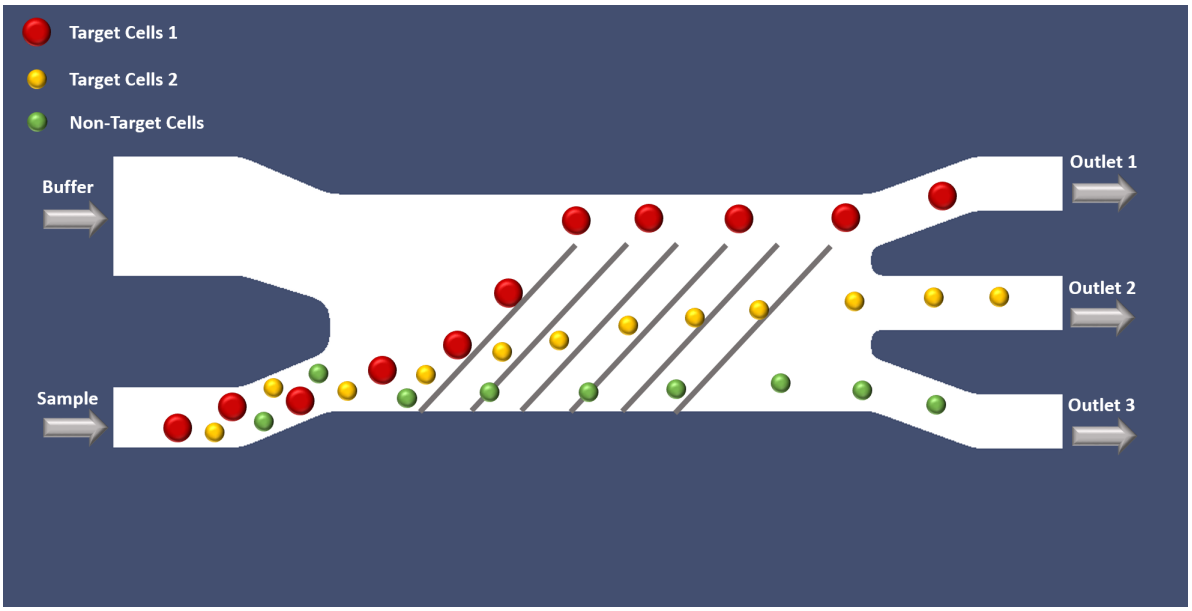

Figure 1.2: A schematic of the dielectrophoretic microfluidic channel

CHAPTER 2

REVIEW OF LITERATURE

2.1 Introduction

Separation and isolation of bioparticles is highly important in many therapeutic and diagnostic applications. Development of lab-on-a-chip (LOC) devices, not only has facilitated the manipulation of cells and other bioparticles, but also offers many advantages such as low cost, small size, low power consumption, and portability, over conventional methods [8]. Recently, Dielectrophoresis has turned out to be an effective and promising technique in manipulating bioparticles which can be used to separate and isolate both charged and neutral particles [18]. What follows is a brief review of research and papers published in the field of Dielectrophoresis.

2.2 AC DEP

In the very classical DEP method, electrodes are employed to produce non-uniform electric fields. Therefore, different bioparticles can be sorted and separated based on their sizes. Payen et al. [19] used dielectrophoresis to separate living mammalian cells from dead cells. They realized that, over a specific frequency range (50-70 KHz) the Clausius-Mossoti factor had a negligible value for living cells, whereas for the dead cells this value was significantly high. Using the fact that the DEP force depends on the Clausius-Mossoti factor, they were able to separate dead cells from living ones. Markx et al. [20] demonstrated that in separating micro-organisms such as bacteria and yeast in low frequencies, the conductivity of medium was of great importance. They were able to separate *E.coli* and *Micrococctls bsodeikticus*. The electrical conductivity of the medium that these micro-organisms were suspended in, had a value in-between the electrical conductivities of *E.coli* and *Micrococctls bsodeikticus*. Doh et al. [21] were able

to separate dead yeast cells from living ones by using a chip with three planar electrodes. The living yeast cells experienced pDEP and were attracted by the electrodes, while the dead yeast cells experienced nDEP and were repelled from the electrodes and stayed suspended in the medium. Megan et al. [22] utilized comb-shaped electrodes to produce high gradient electric fields and trap virus particles. Their work demonstrated that the dielectric properties of the virus depend on the frequency. Thus, at low frequencies the virus experienced pDEP, whereas at high frequencies the virus experienced nDEP. Analyzing cell properties is of great importance in some biomedical fields such as gene introduction or drug injections. Chen et al. [23] applied liquid dielectrophoresis and nDEP in a microfluidic channel to trap a single cell. By proposing a specific design for the channel, they were able to lead a single cell into a cavity and measure its impedance. Similarly, Hameda et al. [24] measured the impedance of bacteria by utilizing pDEP and nDEP at the same time. They implemented some microelectrodes on top of the channel at the entrance region which served as a concentration module. Then, in the downstream of the channel and on the bottom wall, they fabricated another set of microelectrodes to produce pDEP and capture the bacteria. By using both nDEP and pDEP in the channel, they increased the trapping efficiency.

2.3 DC DEP

The difference between AC dielectrophoresis and DC dielectrophoresis is generating non-uniform electric fields by using insulating obstacles. What follows is a brief review on several research done to separate bioparticles using DC dielectrophoresis. Srivastava et al. [7] utilized DC dielectrophoresis to separate different blood types from each other. They created an obstacle along the device by narrowing the width of the channel at some points. The rectangular step created by narrowing the channel generated spatial non-uniform electric field and led to separation of different blood types. Similarly, Kang et al. [6] separated blood cells from cancer cells using DC dielectrophoresis. Their proposed channel

consisted of an insulating hurdle between the inlet and different outlets of the channel. Placing a hurdle in the middle of the channel can produce non-uniform electric fields and separate cells depending on their sizes by applying different voltages to different outlets. In their study, they compared the effect of rectangular hurdles with that of triangular ones. Nakano et al. [25] were able to manipulate proteins using insulated DEP. They generated non-uniform electric fields by placing cylindrical posts all over the channel. Additionally, they replaced cylindrical posts with triangular ones to create higher gradient fields.

2.4 Cancer Cells

One of the applications of dielectrophoresis is separating cancer cells from normal cells. Cancer cells possess different dielectrophoretic properties which makes it possible to separate and isolate them from normal cells. Gascoyne et al. and Becker et al. [26, 27] demonstrated that it is possible to concentrate cancer cells at the edges of the electrodes using pDEP. According to their work, when the frequency changes, the direction of the DEP force applied on the normal and cancerous cells became reversed. In other words, the normal cells experienced nDEP, while the cancer cells experienced pDEP. This led to attraction of cancer cells by the electrodes, and therefore, their separation from normal cells. Similarly, Alazzam et al. [28] separated breast cancer cells from normal blood cells using interdigitated electrodes. Their proposed microfluidic channel consisted of two sets of electrodes. The first set was a pair of diverging interdigitated electrodes. The purpose of this section was to lead both normal and cancer cells to the center of the channel. Therefore, the value of frequency selected for this section was in a range such that both normal and cancer cells experienced nDEP. In the second section of the channel two pairs of converging interdigitated electrodes were manufactured and the frequency was selected in a range such that the normal cells experienced nDEP and were repelled from the converging electrodes, while the cancer cells experienced pDEP and were attracted

by the converging electrodes. Yang et al. [29] separated colorectal cancer cells from normal cells using DEP. Their microfluidic channel consisted of a main channel and a side channel. Two angled electrodes were placed on the bottom of the channel. Under the influence of the peak-to-peak voltage of 16 and frequency of 100 kHz, colorectal cancer cells experienced nDEP. When these cells reached the electrodes, the balance between the DEP force and the hydrodynamic force was in a direction that led the cancer cells towards the side channel, whereas normal cells passed over the electrodes without any deflection. Gupta et al. [30] separated viable cancer cells from blood using pDEP. In their microfluidic device the electrodes were implemented on the bottom of the channel. The sample was injected into the channel through an inlet port which was placed on the bottom of the channel. The injection was done at a low flow rate to keep the particles close to the bottom of the channel where the DEP force was effective on the particles. pDEP acted on the cancer cells and they were attracted to the electrodes on the bottom and were lead towards the outlet port in the downstream of the channel. On the other hand, normal blood cells experienced nDEP and were repelled from the electrodes. These cells were flown to the outlet which was at the exit along the channel.The significance of this research was the ability to collect viable cancer cells and to observe exponential growth of different cancer cells. Alshareef et al. [31] were able to separate two types of cancer cells using DEP. The difference between using DEP and other conventional methods was that, although conventional methods made it possible to detect cancer cells from normal cells, they were not able to locate the origin and type of each cancer cell. Having enough information about the origin of a mass of cancerous cells helps to select the best clinical treatment. Alshareef et al. [31] exploited different behaviour of various cancer cells under the influence of DEP force to separate them from each other.

2.5 Electrode Design and Configuration

DEP force depends on the non-uniformity of an electric field. One of the factors that affects the non-uniformity of an electric field is the design and configuration of the electrodes. Several electrode designs and configurations have been proposed in the literature. What follows is a brief review on different designs and configurations of microelectrodes. Pething et al. [32] used interdigitated castellated microelectrodes to expose yeast cells by both pDEP and nDEP. By changing the frequency and the conductivity of the medium, they were able to sort yeast cells in different patterns. For instance, with frequency of above 10 kHz and conductivity of 5 μScm^{-1}, and similarly, with frequency of above 100 kHz and conductivity of 150 μScm^{-1} for the medium, the yeast cells experienced pDEP and by being attracted to the tips of the electrodes, were formed into pearl-chains. On the other hand, for other frequency and conductivity values, the cells experienced nDEP and were repelled from the tip of the electrodes and formed triangles in the regions between the electrodes. Additionally, some yeast cells, were repelled from the top surface of the electrodes to be away from the high-gradient regions. This group of cells formed diamond patterns on the surface of the electrodes. It is worth mentioning that this configuration was only useful for separation of a batch of particles. Similarly, Morgan et al. [33] created the same patterns for a batch of particles. The difference of their work, however, was that they used planar microelectrode arrays. The problem in this case was that the DEP force decreases with increasing the height of the channel. Therefore, the effect of DEP force was considerable in only a small region above the surface of the electrodes which is why the efficiency of this design was not high enough. Yunes et al. [34] suggested a microfluidic device with two arrays of electrodes on the top and bottom of the channel. The electrodes were designed as chevrons with one side shorter than the other side. The angle between the electrodes and the flow deflected the target particles through the outlet channel. In addition, the chevron shaped electrodes helped

focus the target electrodes away from the wall and towards the outlet. Khoshmanesh et al. [35] designed two arrays of curved electrodes with different purposes. The first set of electrodes were created by intersecting two circles of different radii. The purpose of this array of electrodes was to sort the particles. The second pair was fabricated in the shape of boomerang and were created by intersection of two concentric ellipses. The purpose of the latter set was to assess the sorting of the cells. By producing large DEP forces at the tip and also over a large region along the microelectrodes, sort and separation of large number of particles were made possible. Wang et al. [36] created lateral DEP forces by placing electrodes on the side walls of a channel. These electrodes generated nDEP to repel the particles. The balance between the DEP forces of these electrodes on the two opposing side walls of the channel kept different particles at different positions along the width of the channel and led them through different outlets. This method has the disadvantage of difficulty in fabrication of the electrodes. Jubery et al. [3] proposed a novel microelectrode design to increase the distance between different types of particles. They fabricated a set of trapezoidal electrodes and a set of truncated trapezoidal electrodes on the side wall and bottom wall of the channel. This configuration improved the efficiency of the separation by applying nDEP on the particles in both lateral and vertical directions. This technique also decreased the trapping of the cells on the electrodes and provided an effective continuous separation. Hemmatifar et al. [37] proposed planar triangular electrodes instead of chevron-shaped converging ones. They fabricated two triangular electrodes on the top and two triangular ones on the bottom wall of the channel. This configuration generates higher gradients in the lateral and vertical directions. Voldman et al. [38] proposed another novel electrode configuration. They used four cylindrical extruded electrodes on the bottom of the channel arranged in a trapezoidal configuration. This design was used to trap and confine one type of particle. The problem with this design is its complexity and that it is difficult to fabricate. Chuang et al. [39] proposed a

device which consisted of several different sets of electrodes with different designs and purposes. The first set was a chevron shaped array of electrodes that were converging in the direction of the flow and made the particles focused in the center of the channel. The second set guided the particles towards the trapping electrodes and the third set trapped the particles.

CHAPTER 3

THEORETICAL BACKGROUND

Dielectrohporetic separation is a combination of three phenomena: electric field, fluid flow, and particle motion. DEP force is derived from Guass's law. Fluid flow is governed by Navier-Stokes and continuity equations, and the motion of the particles is defined by Newton's second law of motion. This chapter is an introduction to the theory of each of these phenomena.

3.1 Electric Field

When a charge is in a medium, it affects and changes the properties of its vicinity. If another charge is present in this region as well, it experiences a force which is resulted from the change in the properties of the medium. This change in the properties is caused by the charge's electric field. In other words, electric field can be defined as electric force per unit charge [40]. There is a relationship between electric field and electrical potential ϕ, which is also called the *voltage* [41]. Electric field is defined as:

$$\vec{E} = -\nabla\phi \tag{3.1}$$

In nineteenth century, James Clerk Maxwell proposed that all the fundamentals of electric and magnetic fields can be summarized in four equations. These four equations are Gauss' law for electricity, Gauss' law for magnetism, Faraday's law of induction, and Ampere's law. Since there is no magnetic field involved in this research, only Gauss' law for electricity will be discussed.

3.1.1 Gauss' law for electricity

Gauss' law for electricity is the first of four Maxwell's equations. According to Gauss' law for electricity, electric flux passing through an enclosed surface is proportional to the

total charge of that enclosed surface [41]. The integral form the Gauss' law is as follows:

$$\oint \vec{E}.dA = \frac{\rho_E}{\varepsilon} \tag{3.2}$$

Where $\vec{E}$ is the electric field (V/m^2), $\oint E.dA$ is the electric flux, ρ_E is the net free charge density (C/m^3), and ε is the permittivity of the medium [41].

By applying the divergence theorem on Eq. 3.2, the differential form of the Gauss' law will be obtained as:

$$\nabla.\vec{E} = \frac{\rho_E}{\varepsilon} \tag{3.3}$$

Gauss' law can also be defined as:

$$\nabla.\vec{D} = \rho_E \tag{3.4}$$

Where $\vec{D}$ is the electric displacement or electric flux density (C/m^2). $\vec{D}$ is defined as [41]:

$$\vec{D} = \varepsilon\vec{E} \tag{3.5}$$

3.1.2 Poisson and Laplace equations

By simplifying Gauss' law and in the absence of a time-varying magnetic field, Poisson and Laplace equations are obtained. By considering Eq. 3.4, and knowing that $\vec{D} = \varepsilon\vec{E}$, and by substituting the electric field as the gradient of the electrical potential, Poisson equation can be written as [41]:

$$-\varepsilon\ \nabla^2\phi = \rho_E \tag{3.6}$$

If ρ_v is assumed to be zero, Laplace equation is obtained and defined as:

$$\nabla^2\phi = 0 \tag{3.7}$$

Laplace equation is the case for electrolyte solutions that are far away from the walls of the channel [41].

3.2 Fluid Flow

Incompressibility is a term given to fluid flow with very small density gradients. In other words, in an incompressible flow the density is considered to be constant. In addition, transfer of kinetic energy to internal energy can be ignored and the flow can be assumed to be isothermal [41]. Therefore, the governing equations for incompressible laminar fluid flow are continuity (conservation of mass) and Navier-Stokes (conservation of momentum) equations [41]. In the case of a flow with very low Reynolds number, such as flow in microfluidic devices, the Navier-Stokes equation can be further simplified into Stokes equation.

3.2.1 Continuity equation

Continuity equation states that the mass of an isolated system is conserved over time. Continuity equation is defined as:

$$\frac{d\rho}{dt} + \nabla.(\rho\vec{u}) = 0 \tag{3.8}$$

where ρ is the fluid density, and $\vec{u}$ is the velocity of the fluid [41]. For an incompressible flow the change in the density can be neglected and Eq. 3.8 is reduced to:

$$\nabla.\vec{u} = 0 \tag{3.9}$$

3.2.2 Navier-Stokes equation

The Navier-Stokes equation states that the momentum of an isolated system is conserved over time. For an incompressible flow the Navier-Stokes equation can be written as:

$$\rho \frac{\partial \vec{u}}{\partial t} + \rho \ \vec{u}.\nabla \vec{u} = -\nabla p + \mu \ \nabla^2 \vec{u} \tag{3.10}$$

where ρ is the fluid density, $\vec{u}$ is the fluid velocity, p is the pressure, and μ is the dynamic viscosity of the fluid [41].

3.2.3 Stokes equation

For a flow with low Reynolds number, the Stokes equation can be driven from the Navier-Stokes equation by neglecting the unsteady and convective terms. By dividing Eq. 3.10 by $\mu U/l$ and normalizing the pressure we will obtain:

$$Re \frac{\partial \vec{u}^*}{\partial t^*} + Re \ \vec{u}^*.\nabla^* \vec{u}^* = -\nabla^* p^* + \nabla^{*2} \vec{u}^* \tag{3.11}$$

where Re is the Reynolds number and is defined by $Re = \rho U l/\mu$. If Re is so low that it can be approximated as zero, the unsteady and convective terms are neglected and the Stokes flow is expressed as:

$$\nabla p = \mu \ \nabla^2 \vec{u} \tag{3.12}$$

The Stokes flow equation can be used when $Re < 0.1$ [41].

3.3 Force Analysis

When an electric field is applied, the motion of the colloidal particles through the microfluidic channel is affected by several forces among which dielectrophoretic force, hydrodynamic drag force, and gravitational force are the dominant one. Depending on the Reynolds number and the size of the particles, the lift force and Brownian motion can also be taken into account and influence the motion of the particles [42]. It is possible to optimize a separation process by identifying the dominant forces acting on the particles. According to second law of Newton, the force balance can be written as:

$$m_p \frac{d\vec{u}_p}{dt} = \vec{F}_{DEP} + \vec{F}_d + \vec{F}_g + \vec{F}_B \tag{3.13}$$

where m_p is the mass and $\vec{u_p}$ is the velocity of the particles, and $\vec{F}_{DEP}$, $\vec{F}_d$, and $\vec{F}_g$ are the dielectrophoretic force, hydrodynamic drag force, and gravitational force, respectively. Additionally, F_B takes the effect of Brownian motion into account [43].

3.3.1 Dielectrophoretic force

The most dominant force in a dielectrophoretic separation device is the DEP force. The DEP force is resulted from the interactions between non-uniform electric field and polarizable colloidal particles. By applying an electric field to the colloidal particles, polarization occurs, which is defined as the accumulation of the charge at the interface of the particle and the medium. Due to the difference between the dielectric properties of the medium and the particles, a negative charge on one side of the particle and a positive charge on the other side is created which induces a dipole moment on the particle. Therefore, a net force, known as the DEP force, is exerted on the particles [8]. The DEP force for a spherical particle can be expressed as:

$$\vec{F}_{DEP} = 2\pi\varepsilon_m a^3 f_{CM} \nabla E^2 \tag{3.14}$$

where ε_m is the permittivity of the medium, a is the radius of the particle, f_{CM} is the Clausius-Mossotti factor, and E is the electric field [8].

The Clausius-Mossotti factor is defined as:

$$f_{CM} = \left(\frac{{\varepsilon_p}^* - {\varepsilon_m}^*}{{\varepsilon_p}^* + 2{\varepsilon_p}^*}\right) \tag{3.15}$$

where ε^* is the complex permittivity and can be written as:

$$\varepsilon^* = \varepsilon - \frac{j\sigma}{\omega} \tag{3.16}$$

where j is the imaginary part, ω is the angular frequency of the AC field, and σ is the conductivity [18]. At high frequencies ($\omega \to \infty$), which is the case in this research, the imaginary part of the Clausius-Mossotti factor is negligible and only the real part affects the DEP force [44]. Therefore, the further simplified DEP force can be expressed as:

$$\vec{F}_{DEP} = 2\pi\varepsilon_m a^3 Re(f_{CM})\nabla E^2 \tag{3.17}$$

where $Re(f_{CM}) = (\frac{\varepsilon_p - \varepsilon_m}{\varepsilon_p + 2\varepsilon_p})$, and ε_m and ε_p are the permittivity of the medium and the particle, respectively. When the particle permittivity is greater than that of the medium, $Re(f_{CM}) > 0$, and the particles are attracted towards the regions with high gradient electric field. This phenomenon is known as positive DEP (pDEP). On the other hand, when the permittivity of the medium is higher than that of the particles, the particles are repelled from the regions with high gradient of electric field. This phenomenon is known as negative DEP (nDEP) [18]. As discussed before, usually in dielectrophoretic separations, AC voltages and fields are used. The AC voltage has a sinusoidal behavior, which means that its value changes from zero to the positive peak, from positive to zero, from zero to negative and from negative peak back to zero again. Therefore, an average value must be chosen for voltage to use in field calculations. To find the average value of an AC voltage, the RMS or "Root Mean Squared" method is used. The root mean square of an AC voltage is the square root of the mean value of the squared values of the peak-to-peak voltage (V_{p-p}), and it is obtained by:

$$V_{rms} = \frac{1}{\sqrt{2}}\, V_{p-p} \tag{3.18}$$

where V_{p-p} is the peak-to-peak voltage of the AC field, and V_{rms} is the average value of a DC voltage that would produce the same power dissipation as an equivalent AC voltage [45]. V_{rms} is then used to find the average values of the AC electric field. Hence, Eq. 3.17

becomes:

$$\vec{F}_{DEP} = 2\pi\varepsilon_m a^3 Re(f_{CM})\nabla E^2{}_{rms} \tag{3.19}$$

3.3.2 Drag force

Drag force is exerted on the colloidal particles due to viscous interactions between the medium and the particles. According to Stoke's law, the relation for the drag force can be obtained by:

$$\vec{F}_d = 6\pi\mu a(\vec{u_p} - \vec{u_f}) \tag{3.20}$$

where μ is the dynamic viscosity, a is the radius of the particle, and $\vec{u_f}$ and $\vec{u_p}$ are the fluid and particle velocities, respectively.

3.3.3 Gravitational force

Gravitational force can be expressed as:

$$\vec{F}_g = u_p\ (\rho_p - \rho_f)\ \vec{g} \tag{3.21}$$

where ρ_p and ρ_f are the density values of the particle and fluid ,respectively; and g is the gravitational constant [43]. In this study, because the density of the particle is close to that of the fluid has almost the same value, the gravitational force can be considered negligible.

3.3.4 Brownian motion

The collision between the colloidal particles and the molecules of the fluid generates random motions known as Brownian motion. The mean squared displacement of the particles caused by the Brownian motion can be expressed in terms of the diffusivity (D) as [41]:

$$\bar{x^2} = 2D\Delta t \tag{3.22}$$

where Δt is the time elapsed. The diffusivity for small particles can be obtained using the Stokes-Einstein relation for a sperical particle and it is as follows [41]:

$$D = \frac{K_B T}{6\pi\mu a} \tag{3.23}$$

where K_B is the Boltzmann's constant, T is temperature, μ is viscosity, and a is the particle radius.

In general, when the particle size is so small that it is comparable to the size of the fluid molecules, Brownian motion must be considered in balancing the different forces acting on the particle. In other words, according to Eq. 3.24, if the diameter of the particle is smaller than the critical value, Brownian motion must be taken into account and the second law of Newton is not applicable to balance the forces anymore [43].

$$|F|\ d_p \leq k_B T \tag{3.24}$$

where $|F|$ is the magnitude of all the forces acting on the particle, and d_p is the diameter of the particle. It is worthy of mention that Brownian motion is usually considerable for particles with sizes in the range of nanometer which is not the case in this research.

3.4 Force Balance

Figure 3.1 represents the top view of a dielectrophoretic channel and the dominant forces acting on the particle. The particle moves in the direction of the red arrow which is a resultant of dielectrophoretic and hydrodynamic forces. Hydrodynamic force is a term applied to the forces applied by the fluid motion. In addition, due to small volume concentration of the particles in this study, the particle-particle interaction, and the particle-fluid interaction can be neglected [46].

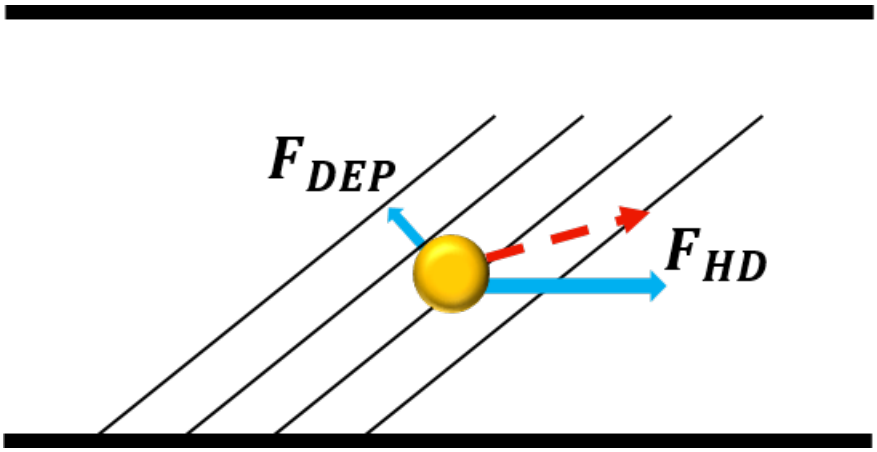

Figure 3.1: Top view of a dielectrophoretic channel with dominant forces acting on the particle

CHAPTER 4

COMPUTATIONAL METHODOLOGY

4.1 Geometry and Boundary Conditions

The microfluidic device is a rectangular channel with an array of slanted electrodes placed on the top and bottom walls. The electrodes have an angle of 10° with respect to the direction of the flow. For the electrodes, boundary conditions were set to a uniform value for voltage on the surface of the electrodes, and uniform value of zero for the walls of the channel. Boundary condition for charge density was set to zero gradient on the walls of the channel and surfaces of the electrodes. For the fluid velocity, boundary conditions at the walls were set to no-slip. The initial velocity at the inlet of the channel varies from 2 mm/s to 6 mm/s depending on the flow rate. For the pressure, boundary conditions were set to zero gradient at the walls, and to uniform value of zero at the outlet of the channel. In order to simulate the process of separation, three different cases were solved. The fluid flow and the electric field were first solved in two separate computational domains. Then, the data obtained from these cases were used to model the particle trajectory in a third domain. The computational channel has the dimensions of 14mm $\times$ 40μm $\times$ 1400μm. The small hydraulic radius of the channel along with the small inlet velocity result in a fully developed laminar flow inside the channel. In this study, because the electrodes are slanted, it is difficult to solve for the fluid flow using the similar geometry. Hence, the fluid flow was solved in a separate domain with straight electrodes and then the results were transferred to the main channel to find the particle trajectories. The electric field can be simply solved for the main domain without changing the geometry of the electrodes. For all three cases, the mesh is clustered near the surface of the electrodes, but uniform elsewhere. Table 4.1 and 4.2 represent some information about each of the three cases including the total number of cells, the mesh type, dimensions, time, and the writing

interval of the data.

Table 4.1: Geometrical parameters of each of the three cases

Case	Mesh Type	Number of Cells	Dimensions
Fluid Flow	Clustered near the surface of the electrodes, Uniform elsewhere	9674000	14mm$\times 40\mu m \times 1400\mu m$
Electric Field	Clustered near the surface of the electrodes, Uniform elsewhere	96740000	14mm$\times 40\mu m \times 1400\mu m$
Particle Trajectory	Clustered near the surface of the electrodes, Uniform elsewhere	9674000	14mm$\times 40\mu m \times 1400\mu m$

Table 4.2: Computational parameters of each of the three cases

Case	End Time	Writing Interval
Fluid Flow	3000 s	1
Electric Field	0.02 s	0.00001
Particle Trajectory	3 s	0.01

Computations for the fluid flow requires a long time to reach the steady state. The electric field, however, due to its static nature, takes a short time to be computed. This chapter describes the computational methodology used to simulate the separation process. In addition, the computer software (OpenFOAM) and its computational methods

along with the mesh generation and the discretization of the governing equations will be discussed.

4.2 OPENFOAM

Open Field Operation and Manipulation, known as OpenFOAM [47], is a free, open source CFD software package which was developed by OpenCFD Ltd. This software contains a broad range of features and packages that have turned OpenFOAM to a powerful tool for solving many complex engineering and science problems. OpenFOAM makes it possible to model and solve fluid flows involving heat transfer, turbulence, and chemical reactions as well as electrostatics and solid dynamics. In addition to that, one of the main advantages of OpenFOAM is that the user has access to the source codes and has the ability to create new solvers or extend the existing solvers by changing the codes. Although free source softwares are generally less accurate than the licensed ones, OpenFOAM has proven to be reliable by being regularly checked and maintained by the developers at OpenFOAM Ltd. Furthermore, much research has been done in different fields of study and in different universities using OpenFOAM. The results obtained from such research are published in well-known journals which indicates the reliability and accuracy of the software. There are several different tools in OpenFOAM including geometry creation and mesh generation tools as well as pre- and postprocessing data analysis. As it was mentioned, one of the greatest benefits of OpenFOAM is having access to the source codes and the solvers. This has turned OpenFOAM into a suitable software in solving multi-physics problems. For instance, dielectrophoretic particle separation is a phenomenon containing different physics such as fluid flow, electric field and particle motion. By using OpenFOAM to simulate this process, it was possible to create a solver to solve for the electric field and to use the predefined solvers to solve for the other two physics and combine them all to create the final case. Parallel computation is another significant advantage of OpenFOAM which helps increase the speed of computation

and reduce the computation time drastically. Depending on the level of the hardware that one's computer has, up to 1000 processors can be used to solve data-intensive problems using OpenFOAM. In other words, OpenFOAM is not limited on the number of processors while other softwares are limited depending on their licenses [48]. There are also some disadvantages associating with OpenFOAM. First and foremost, could be the programming language that this software uses. C++ is an object oriented programming language that resolves the complexity of a problem by building individual software classes (components). These components classify the data and functions, and protect them from accidental corruption [49]. There are very few tutorials and documents for beginners to learn pre- and post-processing and computing problems in OpenFOAM. Solving a multi-physics problem requires time and patience to carefully examine relevant tutorials of each phenomenon and to apply proper modifications to each solver. Although there are not many tutorials in OpenFOAM, many researchers from all around the world have shared their experiences and ideas in CFD online discussion forums to answer other people's questions and to provide useful information for other researchers. In summary, in choosing the right software package, it is necessary to consider the type of problem and the resources. With all the challenges associating with OpenFOAM, once you know how to use it, OpenFOAM is a great software in simulating multi-physics problems.

4.3 Finite Volume Method

In order to discretize differential equations and to solve them in a discretized solution domain, OpenFOAM uses Finite Volume (FV) method. Discretization of the domain is described as dividing the domain into a finite number of discrete regions known as Control Volumes. These control volumes create a computational mesh where the discretized equations are solved. In table 4.1 the mesh information is provided. FV method employs a volume integral form of the problem along with a finite partitioning set of volumes to approximate the discretization of the equations. Volume integrals contain a divergence

term. Therefore, by applying the divergence theorem, these volume integrals are converted to surface integrals. These surface integrals are considered as fluxes at the surfaces of each finite volume. Since the flux entering a given volume is equal to the flux leaving the naighboring control volume, the FV method is known to be conservative [50]. Global governing equations are obtained by writing the governing equations for each control volume and by cancelling out the surface integrals.

4.3.1 Discretization of the Navier-Stokes equation

The Navier-Stokes equation is regarded as a convection-diffusion equation which also contains a source term. The source term is the negative gradient of the pressure. In general, the convection-diffusion equation, also known as the generic transport equation, combines the convection and diffusion terms and describes the transfer of mass, momentum, and energy inside a domain. In this section, the methods used to discretize convection, diffusion, and the source term are demonstrated. Furthermore, because this study is a steady state problem, the time-dependence term will not be considered. The continuity and Navier-Stokes equations are as follows:

$$\nabla.\vec{u} = 0 \tag{4.1}$$

$$\rho \frac{\partial \vec{u}}{\partial t} + \rho \ \vec{u}.\nabla\vec{u} = -\nabla p + \mu \ \nabla^2\vec{u} \tag{4.2}$$

To describe the conservation of a quantity, the coordinate-free vector form of the transport equation, ϕ, is defined as:

$$\frac{\partial(\rho\vec{\phi})}{\partial t} + \nabla.(\rho\nu\vec{\phi}) - \nabla.(\Gamma_\phi\nabla\vec{\phi}) = S_\phi(\vec{\phi}) \tag{4.3}$$

where, from left to right, the terms are known as unsteady term, convection term, diffusive term, and source term, respectively. Also, Γ is defined as the diffusivity of ϕ. To

discretize the equation, the integral form must be used, which is [50]:

$$\int_S \rho\vec{\phi}\nu.ndS = \int_S \Gamma\nabla\vec{\phi}.ndS + \int_\Omega q_\phi d\Omega \tag{4.4}$$

In order to discretize Eq. 4.4, the domain is divided into a finite number of control volumes (CV). The division is done by choosing a suitable grid and by allocating a computational node to the center of each CV. Then, Eq. 4.4 is applied to each control volume, as well as to the entire domain. By adding up the equations for all the control volumes, the global conservation will be obtained. By applying quadrature formulas and approximating the surface and volume integrals, the algebraic equations will be obtained.

4.3.2 Approximation of surface integrals

Figures 4.1 and 4.2 illustrate Cartesian control volumes in 2D and 3D domains [50].

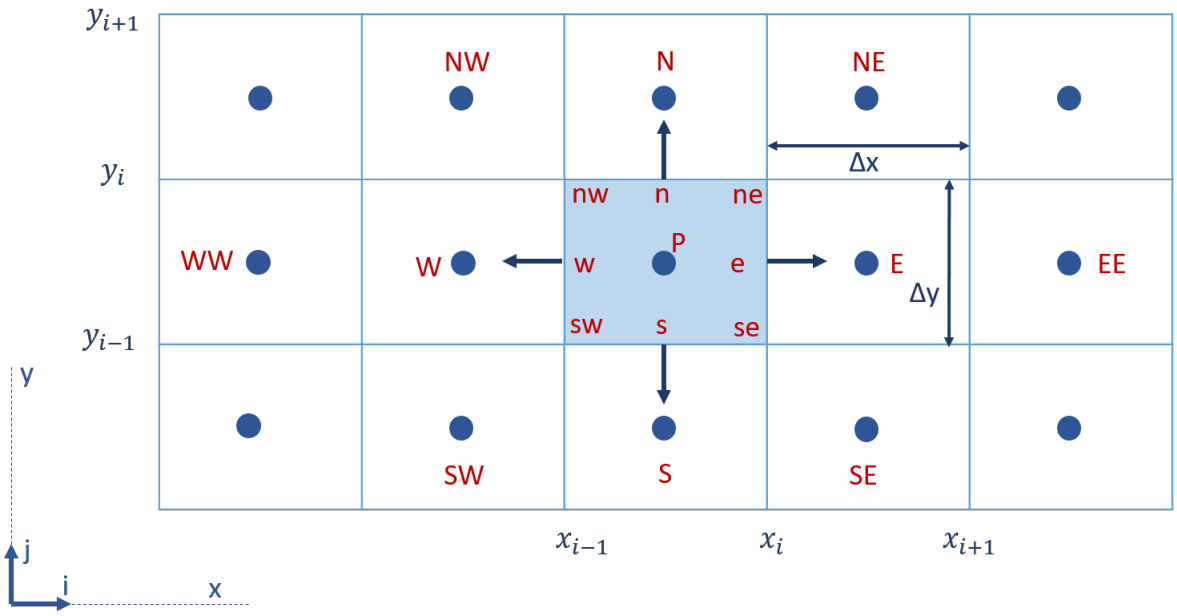

Figure 4.1: A two-dimensional Cartesian control volume

The upper-case letters are denoted to the control volumes and the lower-case letters

are denoted to the surfaces of the control volumes. The lower-case letters are selected depending on their direction. For instance, w denotes west or n denotes north.

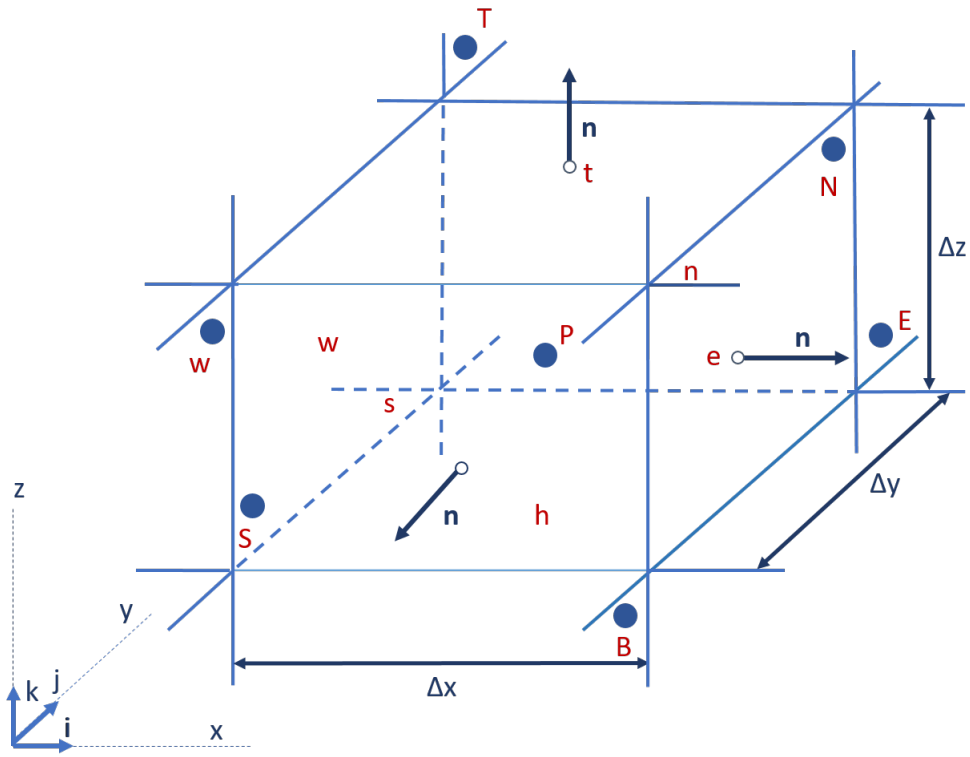

Figure 4.2: A three-dimensional Cartesian control volume

In 2D domains, the control volumes consist of four plane faces whereas in 3D domains they consist of six plane faces. As it was discussed earlier, the surface and volume integrals can be approximated to obtain algebraic equations. By adding up all the surface integrals (four in 2D domains and six in 3D domains), the net flux through the CV boundaries is obtained as [50]:

$$\int_S f dS = \sum_n \int_{S_e} f dS \tag{4.5}$$

where f is either the convective ($\rho\vec{\phi}\nu.n$) or diffusive term ($\Gamma\nabla\vec{\phi}.n$) in Eq. 4.4. In order to simplify the integration of Eq. 4.5, a second order approximation is used. This

approximation, known as the trapezoid rule, is defined as [50]:

$$F_e = \int_{S_e} f dS \approx \frac{S_e}{2}(f_{ne} + f_{se}) \tag{4.6}$$

where f_{ne} and f_{se} are fluxes at the corners of the CV. Using other approximation methods such as Simpson's rule, a fourth-order approximation, may require calculating the flux at more than two corners (here, four corners).

4.3.3 Approximation of volume integrals

In order to simplify the volume integrals, a second-order approximation is used in which the volume integral is approximated by multiplying the mean value of the integrand and the CV volume. In other words:

$$Q_p = \int_{\Omega} q \; d\Omega = \bar{q} \; \nabla\Omega \approx q_p \; \nabla\Omega \tag{4.7}$$

where q_p is the value of q at the center of the control volume [50]. The approximation methods explained in these two sections cannot be applied to some of the terms in the Navier-Stokes equations. Therefore, in the next section, some other approximation methods will be described.

4.3.4 Discretization of convective and viscous terms

The integral and differential form of the convective term in the momentum equation are as follows:

$$\frac{\partial(\rho u_i u_j)}{\partial x_j} \quad , \quad \int_S \rho u_i \nu \; .ndS \tag{4.8}$$

The discretization method used for the convective term in the transport equation can

be applied to the convective term in the momentum equation as well. However, for the viscous term in the momentum equation, the discretization method becomes more complicated due to the fact that the viscous term in the momentum equation is a vector equation [50]. The differential and integral form of the viscous term in the momentum equation are as follows:

$$\frac{\partial \tau_{ij}}{\partial x_j} \quad , \quad \int_S (\tau_{ij} i_j) \ .ndS \tag{4.9}$$

where τ_{ij} is the stress tensor and for an incompressible and Newtonian fluid, it can be expressed as:

$$\tau_{ij} = \ \mu \ (\frac{\partial u_i}{\partial x_j} + \frac{\partial u_j}{\partial x_i}) \tag{4.10}$$

The viscous term in the momentum equation consists of two parts. Eq. 4.11 describes the differential and integral form of the first part of the viscous term as:

$$\frac{\partial}{\partial x_j}(\mu \frac{\partial u_i}{\partial x_j}) \quad , \quad \int_S \mu \ \nabla u_i \ .ndS \tag{4.11}$$

This part of the viscous term can be approximated in the same way as the one in the transport equation. The second part of the viscous term is expressed as:

$$\frac{\partial}{\partial x_j}(\mu \frac{\partial u_j}{\partial x_i}) \quad , \quad \int_S \mu \ (\mu \frac{\partial u_j}{\partial x_i} i_j) \ .ndS \tag{4.12}$$

Eq. 4.12 is non-zero in the case of an incompressible flow. Since, for constant viscosity values, this term is zero, the descretization method will be different and more complicated [50].

4.3.5 Discretization of the pressure term

At this point, an algorithm, known as SIMPLE (Semi-Implicit Method for Pressure-Linked Equations) can be employed as an iterative procedure to solve for the Navier-Stokes equations. The steps of the SIMPLE method are as follows [51]:

1. Assume an initial value for the velocity field to calculate the coefficients in momentum equation.
2. Assume an initial value for the pressure field.
3. Solve the momentum equation to obtain new approximated velocity fields.
4. Generate implementation of H to the pressure equation by using the obtained values in step 3.
5. Calculate the new pressure field by using the values obtained in steps 3 and 4.
6. Correct the velocity field values using an iterative approach based on the new pressure field.
7. Repeat steps 4 through 6 until the solution converges.

4.4 Electric Field Solution

In OpenFOAM, the initial boundary conditions to solve for electrostatic problems are set for ϕ (electric potential) and ρ (charge density). The equation that OpenFOAM uses to solve for the electric field is simply:

$$\vec{E} = -\nabla\phi \tag{4.13}$$

which was earlier discussed in chapter 3.

4.5 Lagrangian Particle Tracking

The numerical method used to track individual particles is known as Lagrangian Particle Tracking. This method is used within an Eulerian phase and is also known as Discrete Particle Simulation. In this method, the position vector of each particle is derived using the following equation:

$$\frac{d\vec{x_p}}{dt} = \vec{u_p} \tag{4.14}$$

where $\vec{x_p}$ is the position of the center of the particle, and $\vec{u_p}$ is the velocity of the particle. It is worthy of mention that particles are assumed to be spherical with diameter D_p and density of ρ_p. According to Newton's second law, the motion of each particle can be governed as:

$$m_p \frac{d\vec{u_p}}{dt} = \sum \vec{F} \tag{4.15}$$

where $\vec{F}$ is the sum of all the forces applying on the particle. Therefore:

$$m_p \frac{d\vec{u_p}}{dt} = \vec{F_{DEP}} + \vec{F_d} + \vec{F_g} \tag{4.16}$$

By substituting the governing equation of each force in Eq. 4.16, the velocity of the particle will be derived as:

$$\frac{d\vec{u_p}}{dt} + a\vec{u_p} = b \tag{4.17}$$

where a and b are constants. Note that $\vec{u_p}$ multiplied by a is derived from substituting the equation for drag force. Eq. 4.17 calculates the velocity of the particle at each time

step. By substituting the value of velocity in Eq. 4.14, the position of the particle at each time step will be obtained.

4.6 OpenFOAM Solvers

OpenFOAM utilizes different linear solvers to solve different discretized equations. Linear solvers are numerical methods used to solve matrix equations. Depending on whether the matrix is symmetric or asymmetric, different solvers are used. In order to solve the equations involved in this project, two different solvers were used. These solvers are the generalized Geometric-Algebraic Multi-Grid (GAMG) solver and the Preconditioned Conjugate Gradient (PCG) solver. The generalized GAMG solver, generates a quick solution on a coarse mesh and maps the results on a finer mesh. Then, it uses these result as an initial guess to obtain an accurate final solution. The priority of GAMG compared to standard methods is the speed of computation since it first solves the equation for a coarse mesh [52]. Preconditioned Conjugate Gradient solver is a method used to solve a system of linear equations with symmetric and positive-definite matrices. This method is used for numerical calculations of partial differential equations that are too complicated to be solved with direct methods. In addition, in OpenFOAM, Smooth solvers are used to literally smooth the solution and reduce the number of errors. The smoother used in this research is the symmetric Gauss-Seidel.

4.7 Mesh Generation

It is not always easy to analytically solve the partial differential equations that govern fluid flow or heat transfer problems. One way to solve such complex problems is to divide the domain into smaller subdomains. As it is illustrated in Figure 4.3, these subdomains are created out of different simple geometries like quadrilaterals and triangles in 2D, and hexahedra and tetrahedra in 3D.

The problem could be solved by discretizing the differential equations in each of these

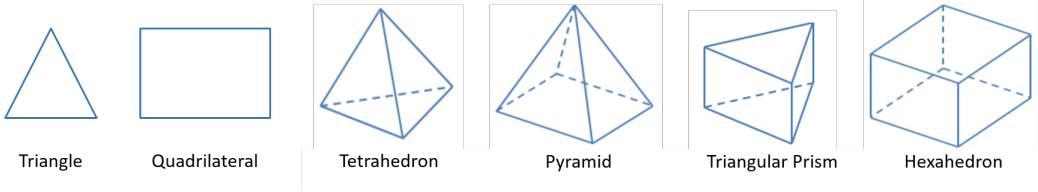

Figure 4.3: Common two-dimensional and three-dimensional cell shapes

subdomains. Each of these subdomains is called a cell, and a collection of these cells is known as a grid or mesh. To achieve an appropriate mesh is termed mesh generation. A fine mesh usually leads to better calculation results. To choose a mesh which provides accurate results depends on various factors such as the convergence rate, the accuracy of the solution and the CPU time. The mesh must be optimized in a way to satisfy these three factors. In other words, the mesh must be coarse enough to decrease the convergence rate and the required CPU time. On the other hand, it must be fine enough to provide results with enough accuracy. It is worthy of mention that regions with high gradient values must have finer mesh to capture all details. Therefore, one way to obtain accuracy along with a short computational time is to increase the mesh density in certain regions with high gradients only, and to have coarser mesh in other parts of the domain [53]. Meshes can be classified into different groups based on the element types or the connectivity of the mesh. Connectivity-based classification categorizes the grid into three types of structured, unstructured, and hybrid meshes. If the connectivity of the mesh is regularly distributed throughout the whole domain, the mesh is known to be structured. A structured mesh can be expressed as a two or three dimensional array. On other other hand, if the grid has an irregular connectivity, it is known to be an unstructured mesh. An unstructured mesh requires a higher storage space compared with the structured mesh. If a grid contains both structured and unstructured portions, it is called a hybrid mesh. In general, using a structured mesh results in highly accurate solutions due to the uniform connectivity between the neighboring cells. It is also requires shorter computational time and less

storage space compared with unstructured mesh. Another way of classifying the meshes is based on the type of the element or the dimensions. In two dimensional problems, most common element types are quadrilaterals and triangles. In three dimensional problems, most popular cell shapes are hexahedra, tetrahedra, pyramids and triangular prisms. Additionally, for structured meshes, if the problem is 2D, quadrilaterals are used, whereas in 3D problems hexahedra are used. In this research, a structured mesh was employed to discretize the computational domain. In modelling the electric field, the surface of the electrodes on the top and bottom walls of the channel creates high-gradient regions. In addition, for the fluid flow the high-gradient regions are near the channel walls. Hence, the mesh in these regions must be fine enough to provide accurate solutions. There are two ways of refining the mesh. One is to increase the total number of cells and the other one is to refine the mesh in high-gradient regions only. In general, increasing the number of cells in high-gradient regions results in a faster and more accurate solution. In this study, electric field requires a finer mesh to solve the equations accurately. Therefore, a grid study was performed to optimize the meshing algorithm with accurate results. As it is shown in Figure 4.4, the mesh is clustered on the surface of the electrodes on the top and bottom walls of the channel and becomes coarser in the center of the channel. It is worthy of mention that, in addition to the surface of the electrodes, the edges have high-gradient fields too. However, since the purpose of using slanted electrodes in this research is to deflect the particles and not to capture them, the interface of electrodes were meshed using a coarse grid. Figure 4.5 is the top view of the channel and the dark blue region is the electrode region. As it is illustrated, the mesh in the entrance and exit regions is not as fine as it is in the electrode region. This is due to the fact that in the entrance and exit region there is a continuous change in the geometry of the cells so that as they reach the electrode region, their sides become parallel to the edges of the electrodes.

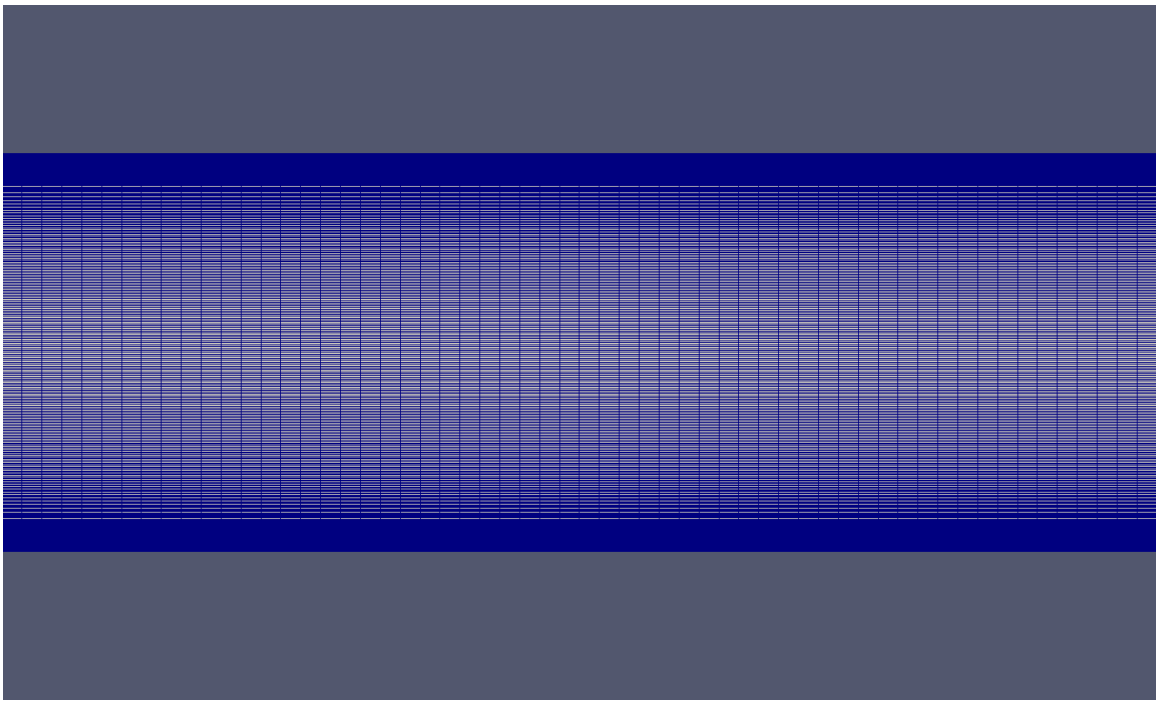

Figure 4.4: Clustered mesh near the surface of the electrodes on the top and bottom walls of the channel, front view

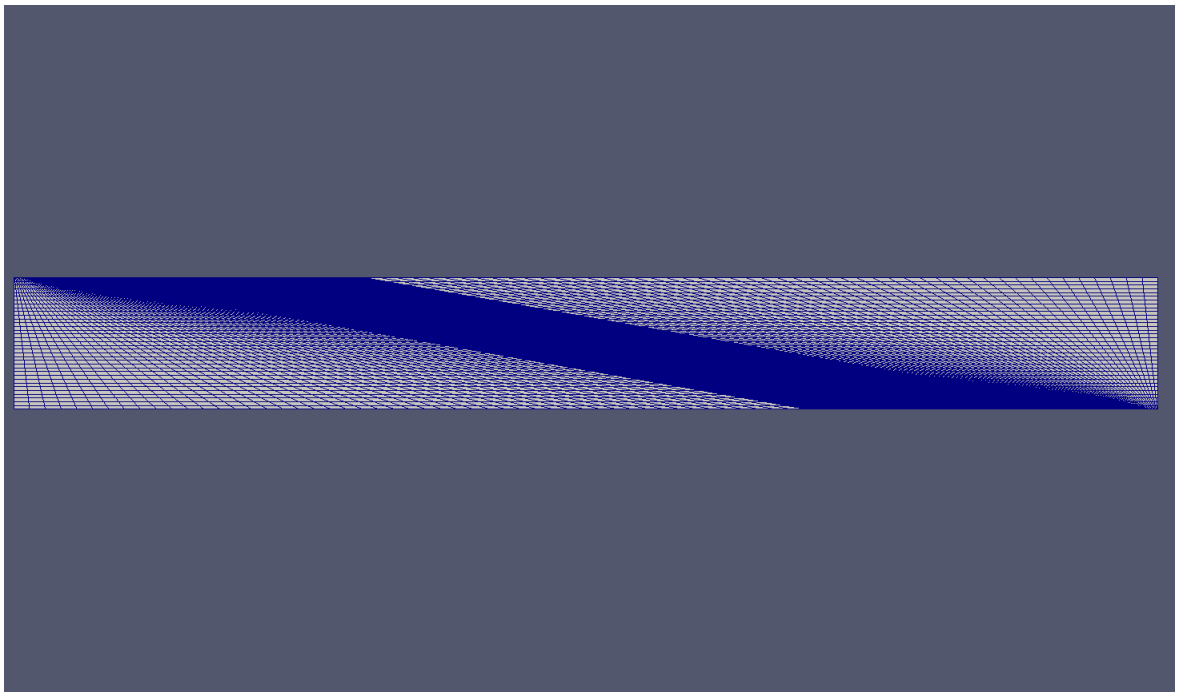

Figure 4.5: Clustered mesh as it reaches the electrode region, top view

4.8 Mesh Independent Study

Mesh independent study is a method to ensure that the selected mesh to perform the numerical simulation is fine enough and that the results obtained from it are accurate and reliable. A super fine mesh (1106×560) was selected and the results obtained from this mesh was considered to be the most accurate and reliable ones. This mesh was the finest mesh that could be generated using the computers in the lab. In order to perform grid study, the super fine mesh was considered to be the reference mesh and the error was calculated with respect to this mesh. It is important to determine the right parameter to perform the grid study for. DEP force is the most important parameter which has a significant effect on the particle motion, and thus, it was selected to do the mesh independent study for. In addition, it is also important to select the right location to do grid study. The centerline of the channel was chosen to perform grid study. Because, as was mentioned earlier, the mesh is clustered near the top and bottom walls of the channel and as it reaches the center, it becomes coarse. Therefore, if the errors calculated for the grid in the center of the channel is low enough, it can be ensured that the DEP force at other locations of the channel is also acceptable. Since the DEP force is negligible in the y-direction, the grid study was done only in the x and z-directions. In what follows, N_x and N_z represent the number of cells in x and z directions, respectively. The grid study was first performed in the x-direction. N_z was kept constant, while N_x was decreased to see its effect on the discretization error. Figure 4.6 shows the effect of decreasing N_x on the discretization error. Several domains with different number of cells in the x-direction were generated and for each of them, the error was calculated with respect to the reference mesh. As can be seen, as the number of cells in the x-direction decreases, the error increases. For $N_x = 691$ and above, the error is less than 1% which is an indication of high accuracy. Additionally, by choosing $N_x = 790$ or $N_x = 921$ the computational time increases which is not desired. Therefore, $N_x = 691$ was chosen as the number

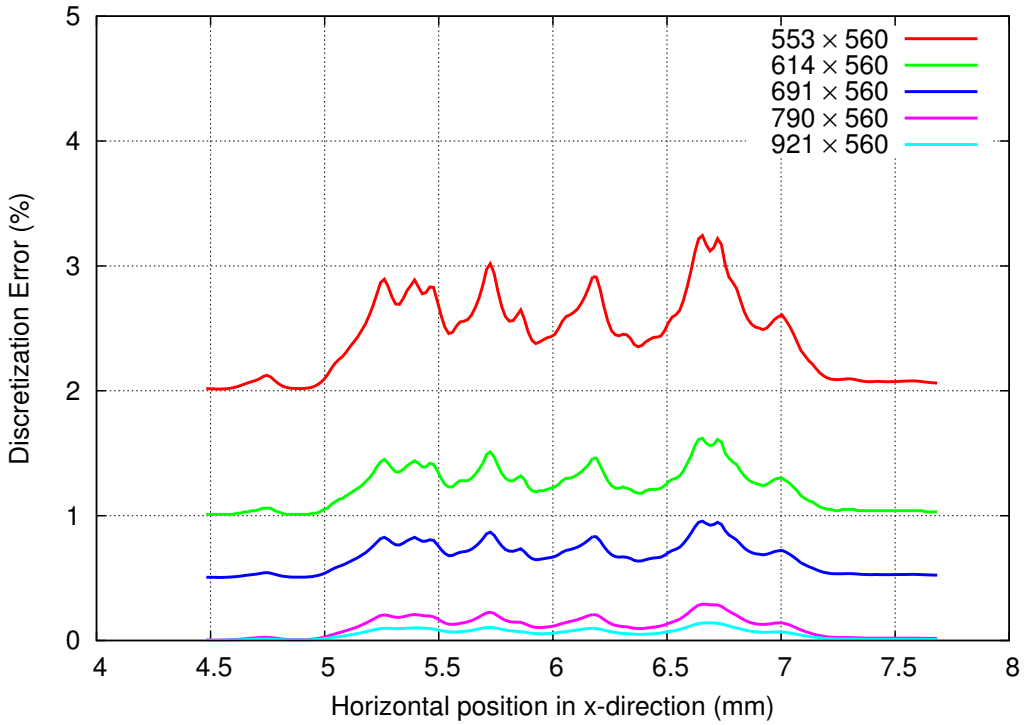

Figure 4.6: DEP force discretization error along x-axis at y=20μm for five different mesh sizes. Grid refinement is in x-direction.

of cells in the x-direction. Next step is to perform the mesh independent study in the z-direction. Therefore, N_x is kept constant and equal to 691, while the error is calculated for different values of N_y. As can be seen in Figure 4.7, by decreasing the number of cells in the z-direction, the error increases to above 1%.Therefore, an appropriate mesh could be generated using either $N_z = 140$ or $N_z = 280$. However, it is also necessary to consider the computational time, which in this research is already high due to the 3D nature of the problem. Hence, $N_z = 140$ was selected as the number of cells in the z-direction. Finally, to achieve the desired accuracy and reasonable computational time, the grid resolution of 691×140 was selected to solve the required partial differential equations within 1% error.

In this study, it was not possible to solve for the fluid flow by placing slanted electrodes. One problem with the solution of the fluid flow in OpenFOAM is that the mesh cells must be orthogonal and uniform. Here, the mesh cells are not orthogonal, since they have

the same shape as the electrodes and their sides are parallel to the sides of the electrodes.

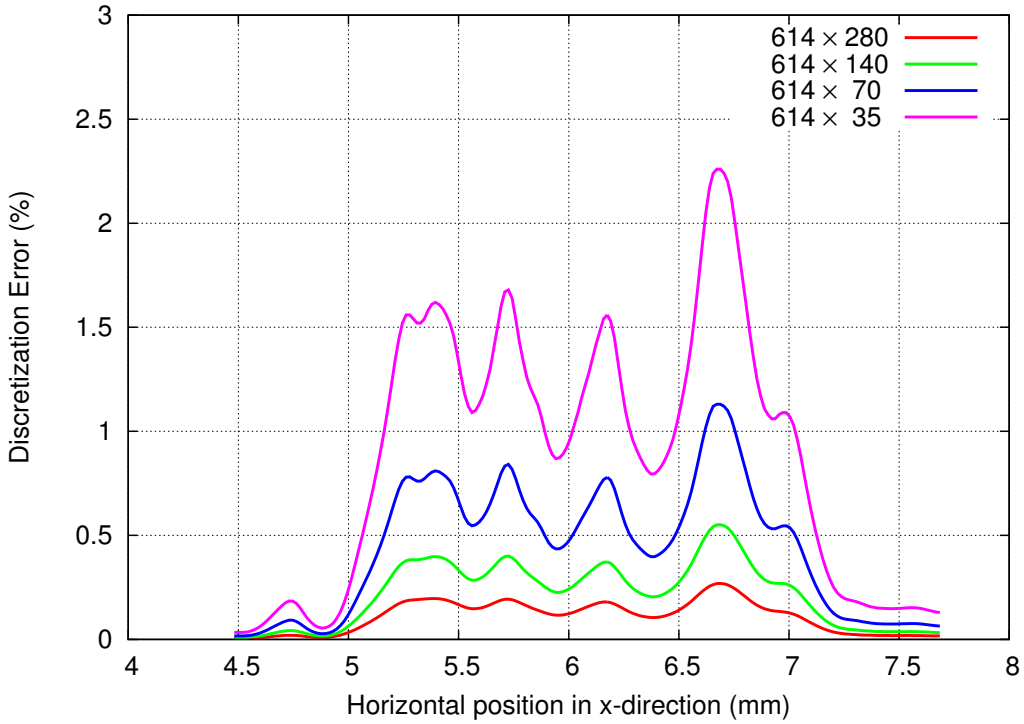

Figure 4.7: DEP force discretization error along x-axis at y=20μm for four different mesh sizes. Grid refinement is in z-direction.

Therefore, to solve this problem, a domain with the same dimensions, but with straight electrodes, was made to solve the fluid flow. Then, the obtained solution for this domain was mapped into the main domain with slanted electrodes. Because the height of the electrodes is only 0.2μm and the flow is laminar, the velocity profile is not expected to be affected by the electrodes. Thus, the velocity profile in a channel with straight electrodes is completely the same as that of a domain with slanted electrodes. To prove this, the analytical solution of poiseuille flow inside a rectangular channel was compared with the results obtained from simulation. Figure 4.8 illustrates both analytical solution and simulation results. As can be seen, the results obtained from OpenFOAM is in good agreement with the analytical solution. In addition, Figure 4.9 depicts the residuals of Navier-Stokes equation and that the pressure and velocity equations are converged.

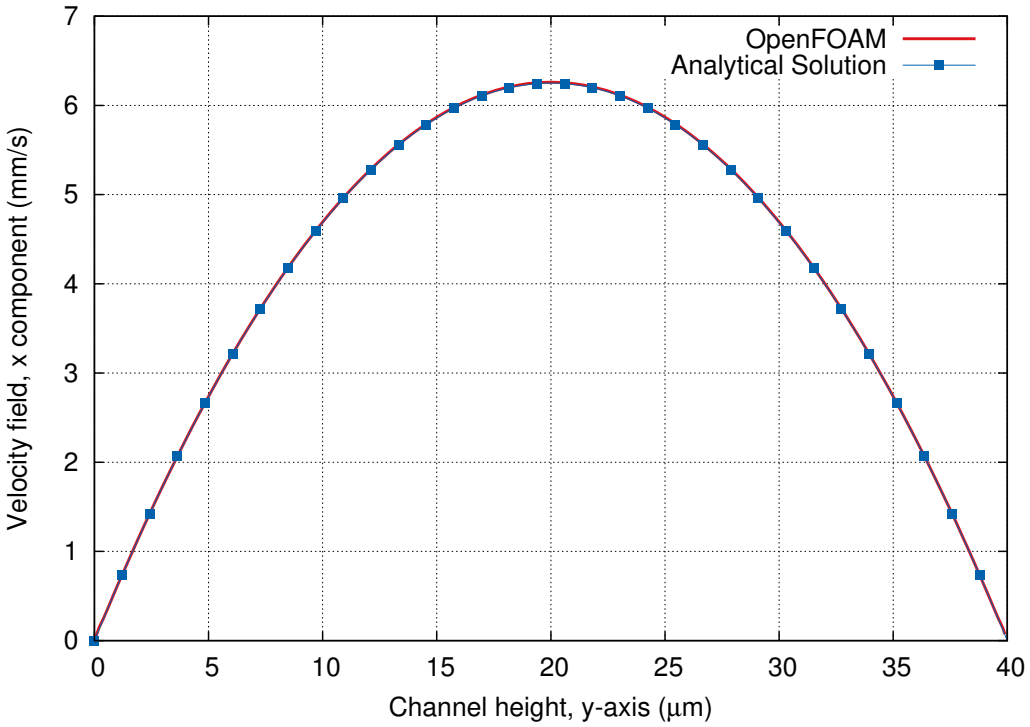

Figure 4.8: The computational results vs. analytical solution for the velocity profile inside the channel in a fully-developed laminar flow case

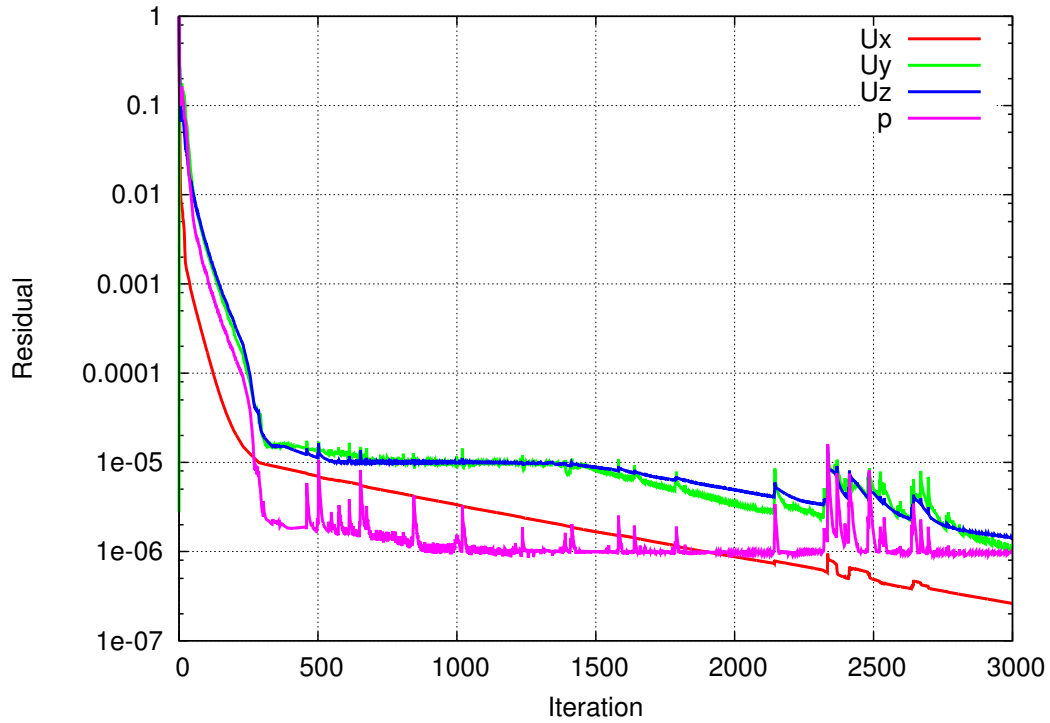

Figure 4.9: Residual monitors for the fluid flow simulation inside the channel.

CHAPTER 5

RESULTS AND DISCUSSION

This chapter presents the results obtained from the computational modeling of the electric field and particle trajectory. The electric field was simulated for an array of slanted electrodes on the top and bottom walls of the channel. By calculating the DEP force, the motion of the particles were also modeled. Furthermore, a parametric study was performed to investigate the effect of different parameters in DEP force and the particle motion. This parametric study includes the effect of flow rate, voltage, number of electrodes, particle size and the height of the channel. The results are further discussed throughout this chapter.

5.1 Electric Field Simulation

The electrodes used in this research are with overall dimensions of $20\mu m \times 8062\mu m \times 0.2\mu m$ and are placed with an angle of 10° with respect to the direction of the flow. In the actual case, the electrodes are placed on top and bottom walls of the channel to eliminate the effect of DEP force in the y-direction. In what follows, first the results obtained from computational modeling of an array of slanted electrodes on the bottom of the channel is presented and then the results for the case with electrodes on top and bottom walls of the channel are discussed.

5.1.1 Electric field for electrodes on the bottom wall

Figure 5.1 illustrates the magnitude of electric field for 10 pairs of slanted electrodes on the bottom wall of the channel. As can be seen, the magnitude of electric field reaches its peak at the edges of the electrodes. The alternating nature of the electric field is due to the change in the value of voltage from one electrode to its adjacent one, and thus the electric field has a cyclic pattern throughout the domain. Additionally, as the distance

from the surface of the electrodes increases, the magnitude of electric field decreases and the peaks become flatter. This is due to the fact that the strength of electric field has its maximum value at the surface of the electrodes and it becomes weaker as the distance from the surface of the electrode increases.

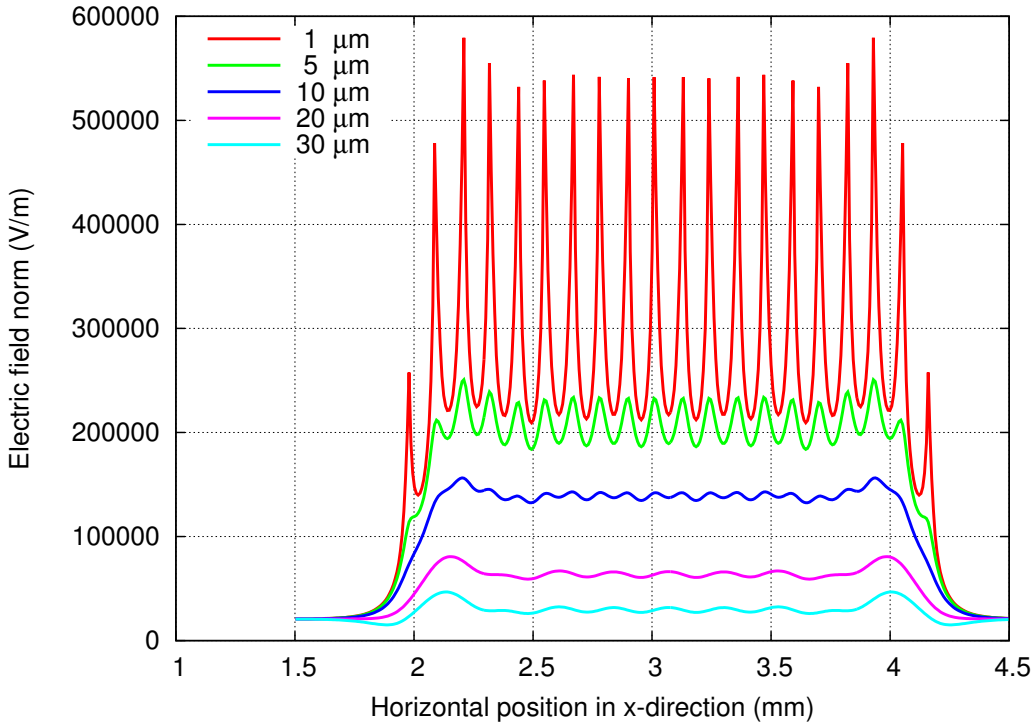

Figure 5.1: Variation of electric field along the channel at different distances from the surface of the electrodes

5.1.2 Electric field for electrodes on the top and bottom walls

Figure 5.2 represents the magnitude of electric field for 10 pairs of slanted electrodes placed on the top and bottom walls of the channel. The electric field is plotted at the centerline of the channel. The electric field at the center of the channel in this case has its minimum value, because the centerline is the farthest distance from the electrodes on top and bottom of the channel. As can be seen, the overall pattern is the same as the previous case and the only difference is in the values. The configuration of the electrodes is in a way that for each positive or negative electrode on the bottom, there is an electrode

with the same voltage on the top which is completely aligned with the bottom one. This configuration creates greater electric fields along the x and z axis compared to the case with an array of electrodes on the bottom wall only. Since the electrodes are completely aligned with each other, the fields resulted from the top electrodes are added to the fields produced by the bottom electrodes, hence creating stronger electric fields. On the other hand, the electric fields in the y-direction generated by the top and bottom electrodes have opposing directions and cancel each other out. Therefore, compared to the x and z directions, the electric field in the y-direction is nearly zero.

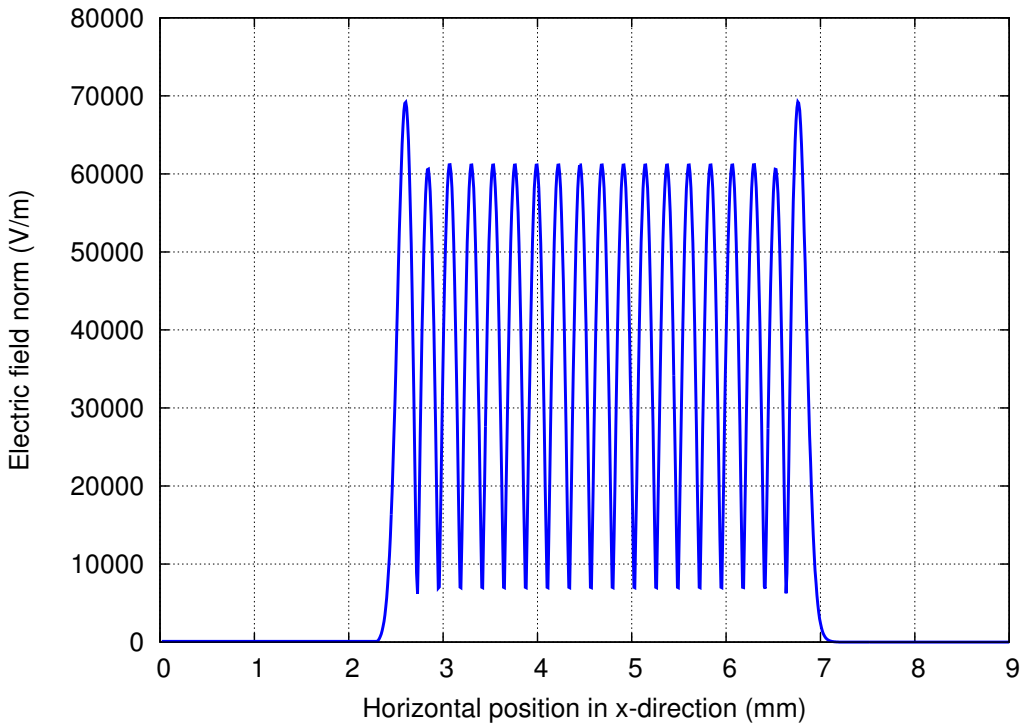

Figure 5.2: Variation of electric field along the channel at different distances from the surface of the electrodes

This configuration maintains the viability of the bioparticles by keeping them in the center of the channel and reducing their contact with the electrodes. Notice that the electric field distribution is symmetric with respect to the centerline. In other words, if the field is plotted $5\mu m$ above the centerline and $5\mu m$ below the it, the graphs are exactly

the same. This pattern can also be seen for the DEP force distribution which is further explained in the next section.

5.2 DEP Force

DEP force is calculated using Eq 3.19. Figure 5.3 illustrates components of DEP force in all three directions. The particle has a diameter of $10\mu m$ and the flow rate is 840 $\mu L/h$. The applied peak-to-peak voltage is 10 V. As mentioned earlier, the y component of DEP force is very small compared to the x and z components and can be approximated as zero. The change in the direction of F_x and F_z is due to change in the voltage value from one electrode to its adjacent one.

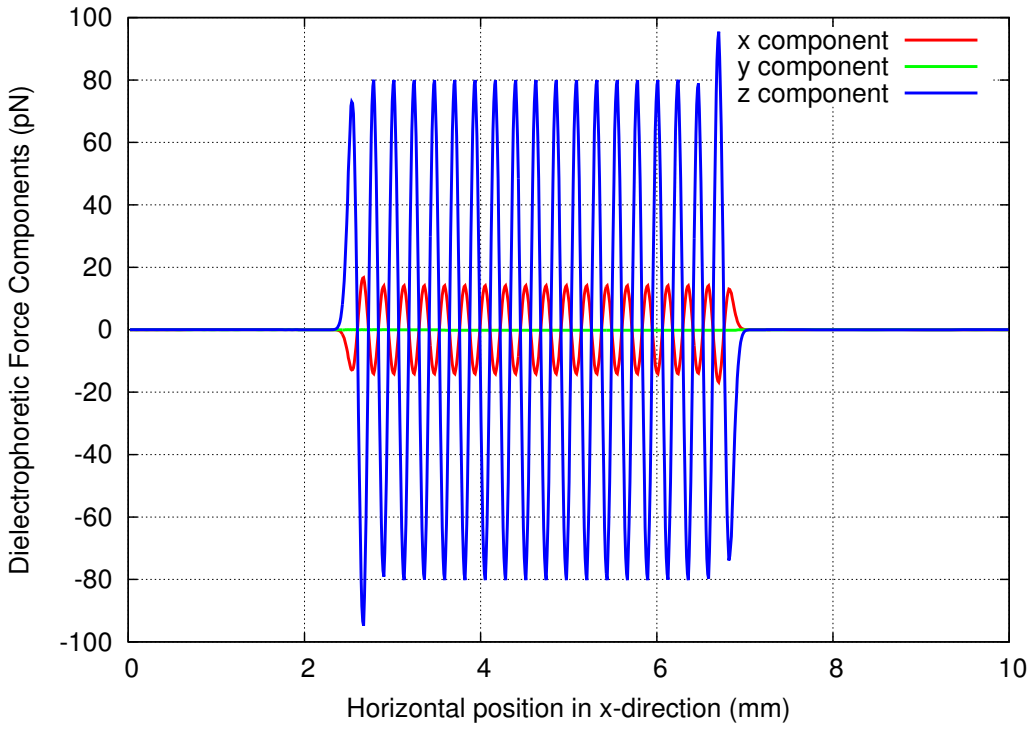

Figure 5.3: x component of DEP force along the channel at the centerline

As can be seen, the z component of DEP force is about four times as much as the x component and is produced by the slanted electrodes. In other words, the primary purpose of using slanted electrodes is to generate enough force in the z-direction which

can deflect the particles and lead them towards different outlet chambers. For further clarification, two extreme cases are explained. If the electrodes are normal to the direction of the flow, the DEP force in the z-direction will be so small that can be approximated as zero and the particles will be influenced only by the x and y components of DEP force. In this case, the particles do not deflect and will move in a straight path along the channel. On the other hand, if the electrodes are placed with an angle of 0° with respect to the flow, the x component of DEP force will be negligible and the particles will be affected by the y and z components of force only. The motion of particles in the latter case is defined by the magnitude of the hydrodynamic force and the DEP force. By decreasing the angle of electrodes with respect to the flow, the z component of the force increases and the particles are deflected in the direction of the magnitude of x and z components of the force.

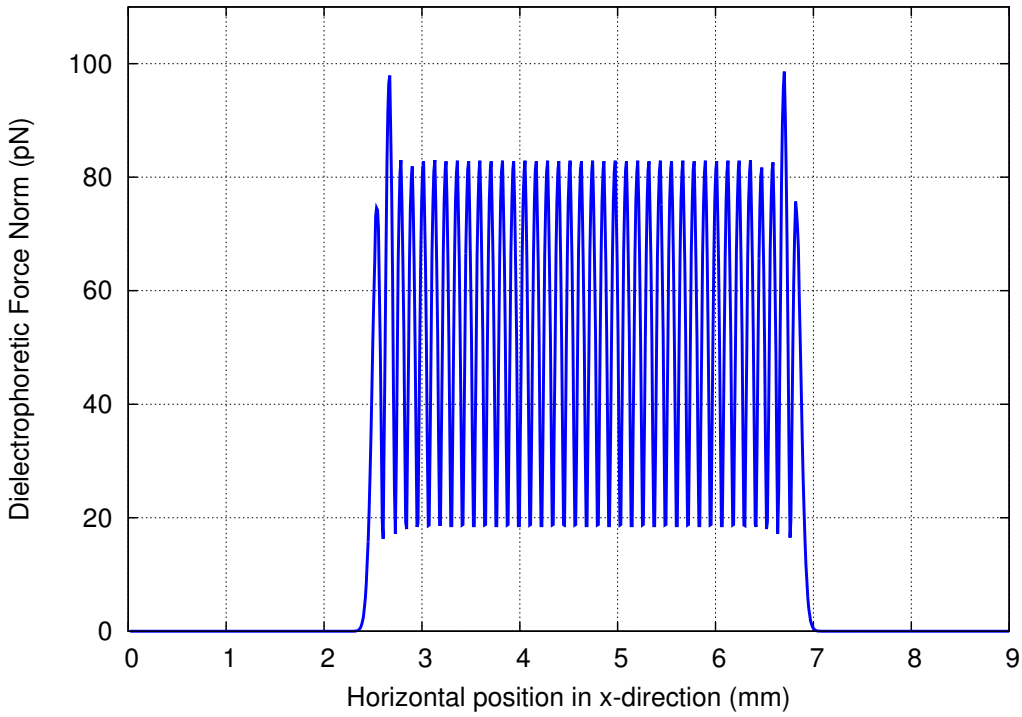

Figure 5.4: Magnitude of DEP force at the centerline of the channel for a particle size of $10\mu m$.

In the current research, the z component of DEP foce has higher values than that of the x component. Considering the two extreme cases with electrode angles of 90° and 0° with respect to the flow, electrode angle of 10° is very close to the latter case where there is only y and z components of the force. Therefore, the z component of DEP force is stronger compared to the x component. Figure 5.4 depicts the DEP force norm along the channel.

5.3 Verification of Computational Results

Verification of the results is of paramount importance in evaluating the accuracy and reliability of a computational simulation. One way to do so, is to perform the actual experiment and to compare the results with those obtained from simulation. However, due to lack of resources and high cost of equipment, it was not possible to conduct the actual experiment in this study. Therefore, two experimental articles were selected and for each of them, the microfluidic device with the same geometry and operating parameters were simulated. Finally, the experimental results were compared and verified with those obtained from numerical simulation. Kim et al. [54] reported a microfluidic device in which both dielectrophoresis and magnetophoresis were utilized to separate three different types of particles. Here, we only modeled the dielectrophoretic section of their channel to verify our results with the experiment. The DEP module of the device is 1400 μm wide and 20 μm high. The length depends on the number of electrodes, and in our case is about 11 mm. The fluid velocity was set to $\approx 11 mm/s$, and the peak-to-peak voltage of 20 V was applied to the electrodes. The electrodes were placed with an angle of 10° with respect to the flow direction. Two particles with diameters of 5 μm were injected into the channel. Although in Kim et al. experiment the size of the non-target particles was 1 μm, we chose a bigger size for the non-target cells for better visibility. Figure 5.5 shows the side view of the same case. The green particle is target and the yellow one is non-target. As can be seen, the green particle begins levitating as soon as it reaches the

first electrode. After it reaches the centerline, it stops levitating because the y component of DEP force is approximately zero at the centerline of the channel. On the other hand, the non-target yellow particle is not affected by DEP force and continues its straight path towards the waste chamber. Figure 5.6, illustrates the top view of the simulated channel. Note that the size of the particles shown in Figures 5.6, 5.5, and 5.7 are not to scale and are enlarged for better visibility. As can be seen, the green particle is deflected as soon as it reaches the first electrode and follows its path along that electrode until it reaches the region with no electrodes. It then continues its straight path towards the collecting chamber. On the other hand, the yellow particle is not affected by DEP force and continues its straight path towards the waste chamber. It is worth mentioning that the parameters were optimized in a way to produce high values of DEP force, which causes the DEP-labeled particles to deflect by the first electrode. In another article, Kim et al. [16] reported a dielectrophoretic separation device which was used to separate cells based on their phases. They exploited the fact that the volume of the cell varies with changes in its phase. We used the same channel geometry and parameters to show that our results were in good agreement with those obtained by Kim et al. The channel is 1400 μm wide and 40 μm high. The fluid velocity was set to $\approx 3mm/s$. The electrodes were placed with an angle of 10° with respect to the direction of the flow and a peak-to-peak voltage of 20 V was applied. Two target particles with diameters of 10 μm and 20 μm were injected into the channel. The purpose of this work was to show that particles with larger diameters deflect more than the ones with smaller diameters. Figure 5.7 shows the top view of the channel. As can be seen, the yellow particle with a diameter of 20 μm is deflected as soon as it reaches the first electrode and moves along that electrode until it reaches the end of the electrode. On the other hand, the DEP force on the green particle is not high enough and it does not experience a significant deflection by the first electrode. This particle enters the electrode region and is deflected slightly by passing

over each electrode. In the end, it exits the electrode region with a total deflection of about 200 μm normal to the flow direction.

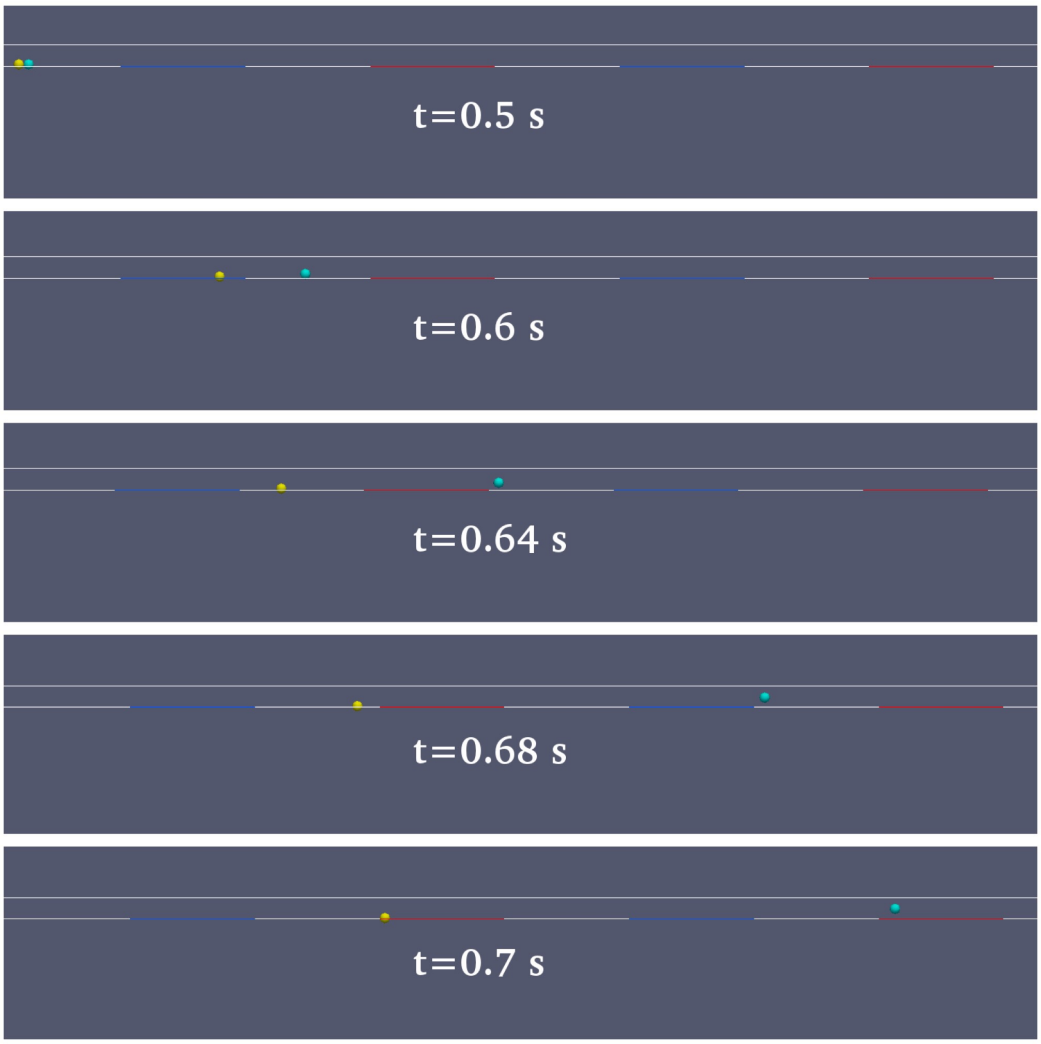

Figure 5.5: Side view of DEP separation process for one target and one non-target cell with diameters of 5 μm. $V_{p-p} = 10\ V$, flow rate=840 $\mu L/h$

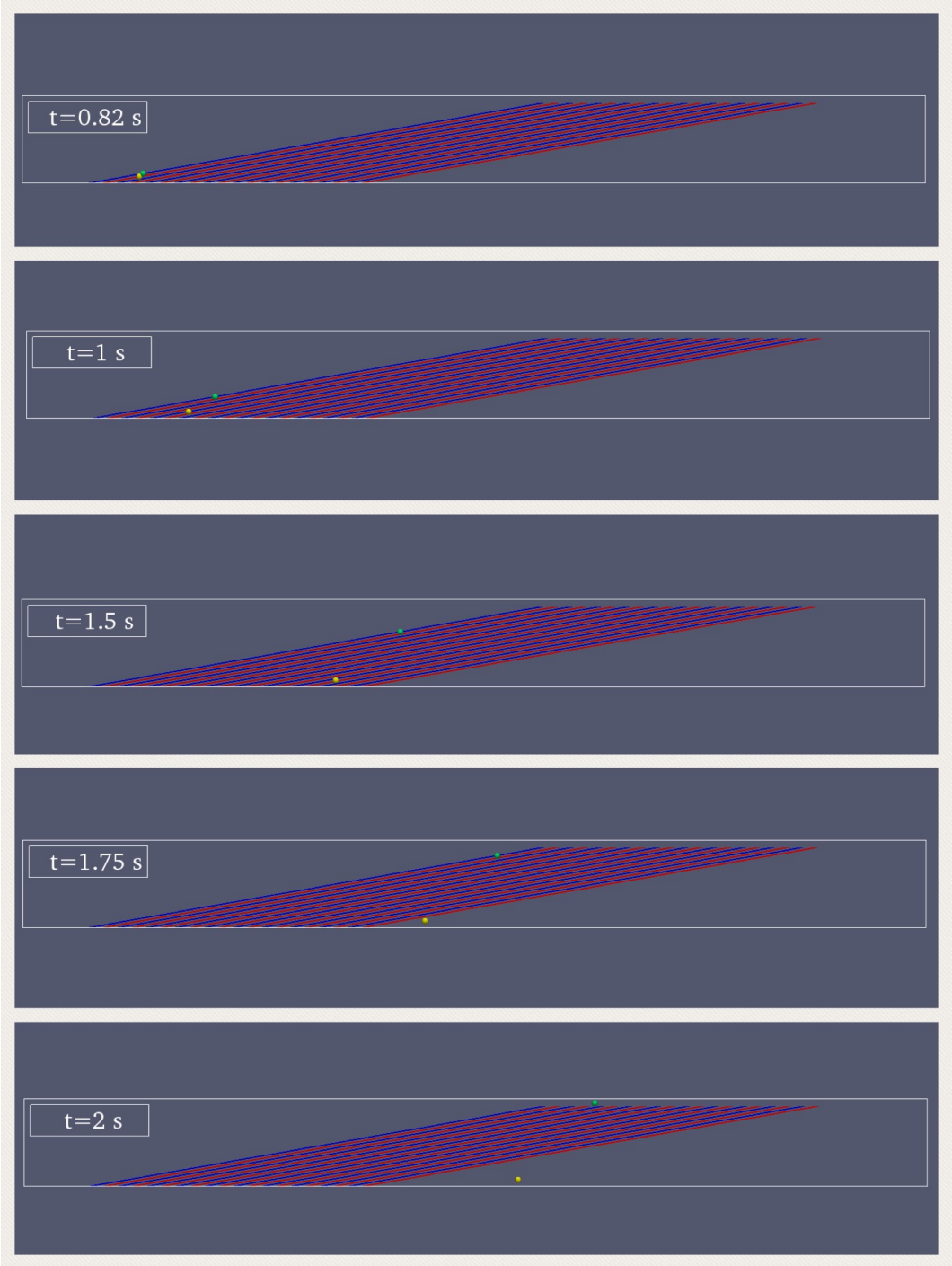

Figure 5.6: Top view of DEP separation process for one target and one non-target cell with diameters of 5 μm. $V_{p-p} = 10\ V$, flow rate=840 $\mu L/h$

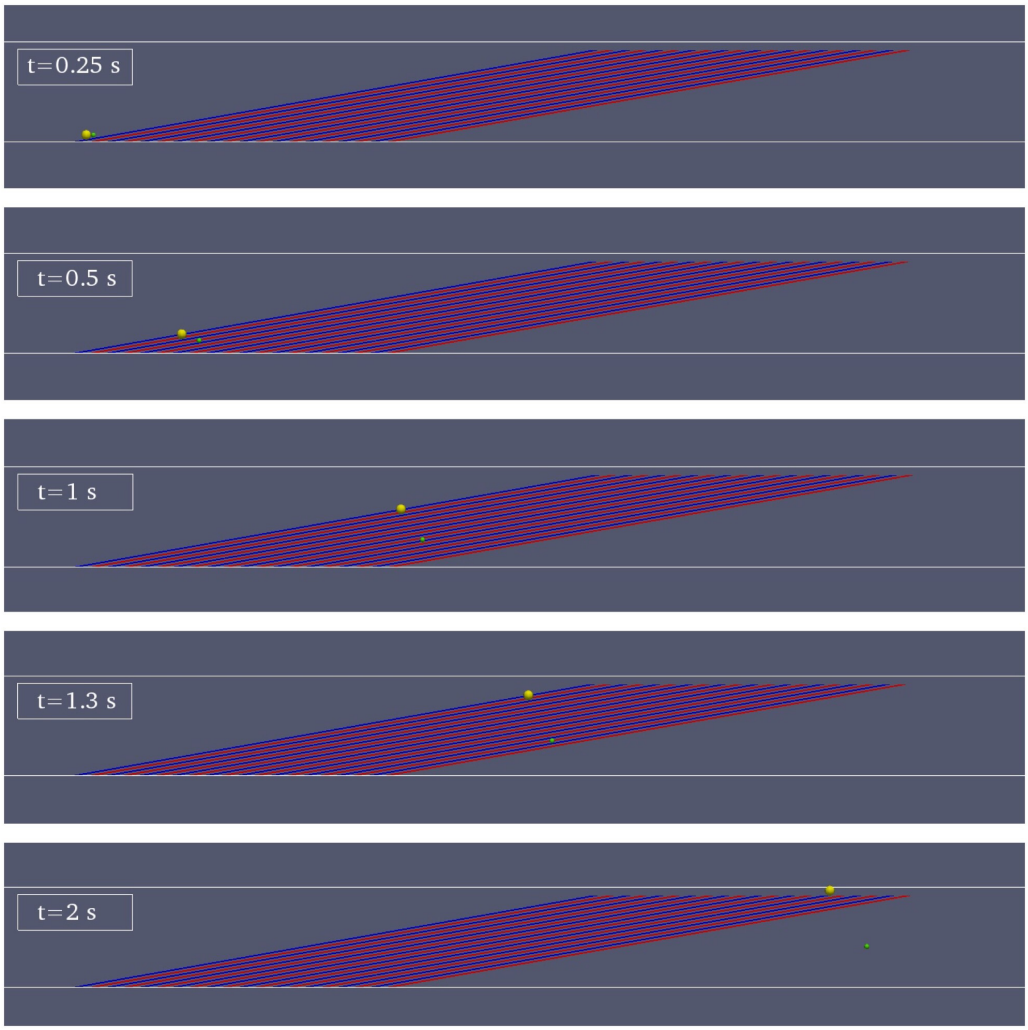

Figure 5.7: DEP separation process for two target cells with diameters of 20 μm and 10 μm (yellow and green, respectively). $V_{p-p} = 10\ V$, flow rate=840 $\mu L/h$

5.4 Parametric Study

Several studies were done to investigate the effect of different parameters on the DEP force and the separation process. The studies were performed for two groups of operating parameters and geometric parameters. The operating parameters include the effect of flow rate, voltage and the particle size, and the geometric parameters include the effect of channel height and number of electrodes.

5.4.1 Flow rate

Figure 5.8 represents the effect of flow rate on the particle trajectory in a dielectrophoretic microfluidic channel. The cell diameter is $10\mu m$ and the peak-to-peak voltage is $10V$in all cases. As was mentioned earlier, the fluid velocity plays an important role in calculating the drag force (Eq. 3.20). Therefore, by increasing the fluid velocity, or in other words, by increasing the flow rate, the drag force increases and a higher DEP force is required to separate the particles. As can be seen in Figure 5.8, at high flow rates, the deflection of the particles is not as much as it is for low flow rates. hence, in order to have enough deflection at high flow rates, the voltage must be increased. However, increasing voltage is limited by the viability of the cells, and much more important than that, by the electrolysis at the electrodes [17].

Additionally, in the case with flow rate of 420 $\mu L/h$ which corresponds to fluid velocity of ≈ 2 mm/s, the DEP force is so strong that the particle is deflected as soon as it reaches the first electrode and does not enter the electrode region at all. By increasing the flow rate to 630 $\mu L/h$, the drag force increases and the particle passes the first electrode, but does not enter the electrode region completely. For the highest flow rate of 1260 $\mu L/h$, the particle is deflected slightly.

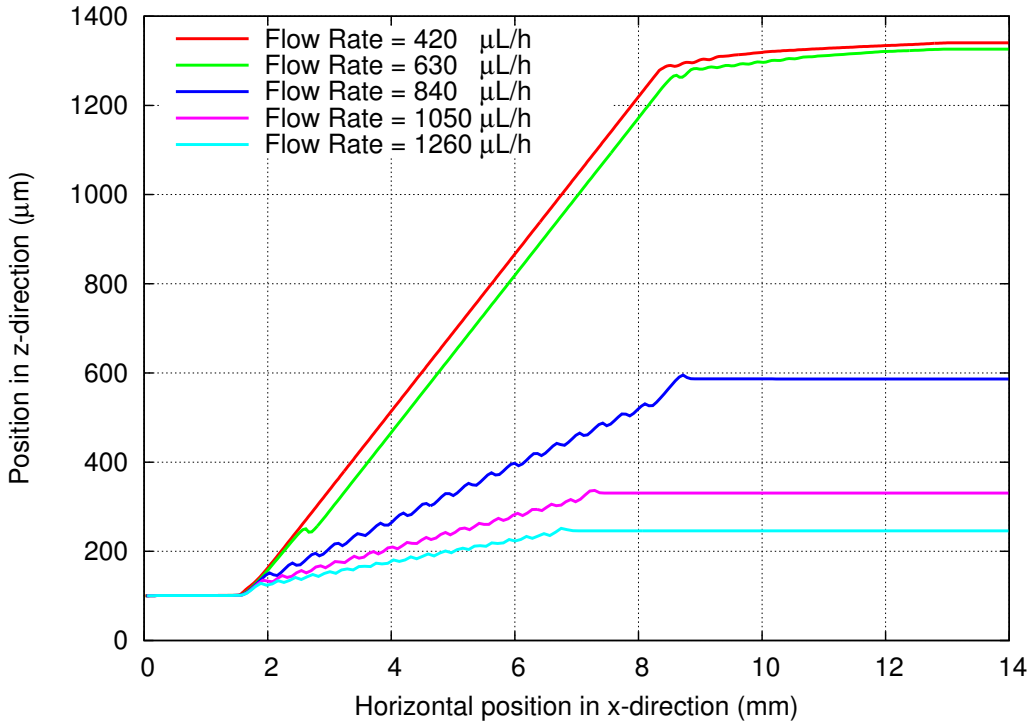

Figure 5.8: Deflection of a $10\mu m$ particle with applied peak-to-peak voltage of $10V$ for different flow rates

5.4.2 Voltage

Figure 5.9 illustrates the effect of voltage on the particle trajectory. The cell diameter is $10\mu m$ and the flow rate is 840 $\mu L/h$ which results in a fluid velocity of ≈ 4 mm/s in all three cases. As can be seen, by increasing the voltage, the DEP force increases and the deflection of the particle reaches its maximum.

For instance, for peak-to-peak voltage of 15 V the DEP force is so strong that the particle is deflected as soon as it reaches the first electrode and moves along the electrode all the way up to the top of the channel where there is a region with no electrodes. By decreasing the voltage, the drag force becomes dominant and the deflection of the particle decreases. It is important to optimize the flow rate and the voltage so that the deflection of the particle is within the optimal range. For instance, the flow rate of 840 $\mu L/h$ is so high for the peak-to-peak voltage of 5 V that the particle has no deflection and flows

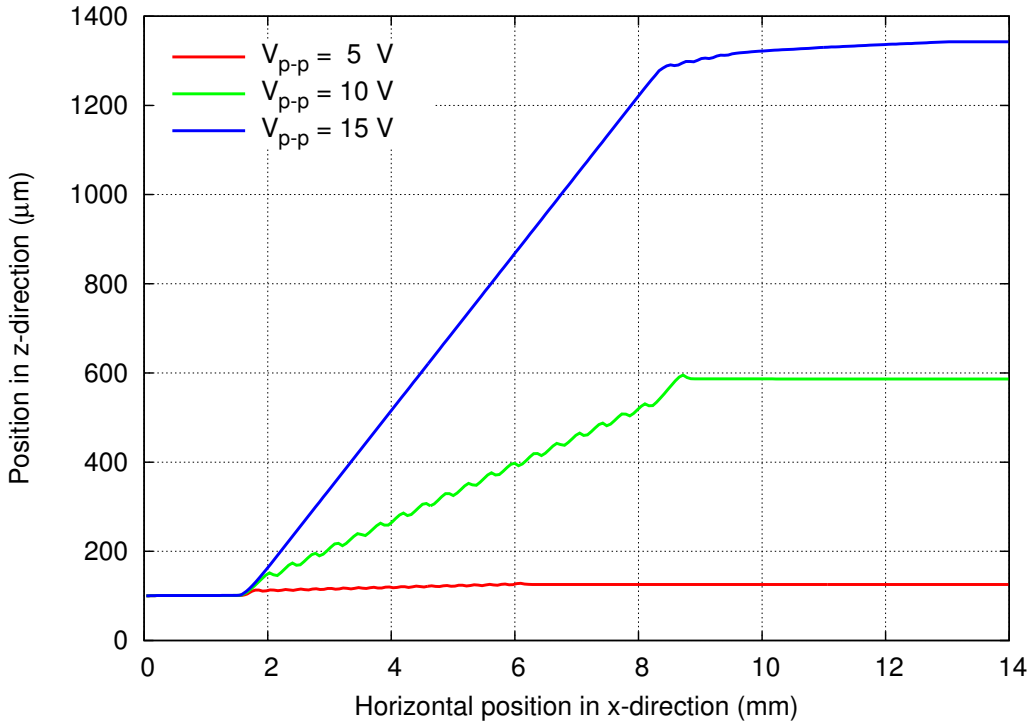

Figure 5.9: Deflection of a 10 μm particle with flow rate=840 $\mu L/h$ for different peak-to-peak voltages

along the channel. On the other hand, this flow rate is enough for the peak-to-peak voltages of 10 and 15 V to deflect the particle into the electrode region. It is worthy of mention that increasing the voltage to higher values than 15 V will result in the same particle trajectory, however, as was mentioned earlier, increasing the voltage is limited by the electrolysis and the viability of the bio-particles.

5.4.3 Particle size

Figure 5.10 shows the trajectory of three particles with different diameters of 5 μm, 10 μm, and 15 μm. For all three cases, the peak-to-peak voltage is 10 V and the flow rate is 840 $\mu L/h$ which results in a fluid velocity of $\approx$ 4 mm/s. As was mentioned previously in Eq. 3.19, radius of the particle plays an important role in calculating the DEP force. By increasing the radius of the particle, the effect of DEP force increases as well. It is worthy of mention that the drag force depends on the radius of the particle. However, the drag

force has a linear relation with the radius, while the DEP force has a cubic dependency on the particle radius. Therefore, by increasing the size of the particle, the DEP force increases and more deflection will be obtained. The particle size is also limited by the height of the channel. If the particle size is too large compared to the channel height, clogging may occur in the microfluidic device.

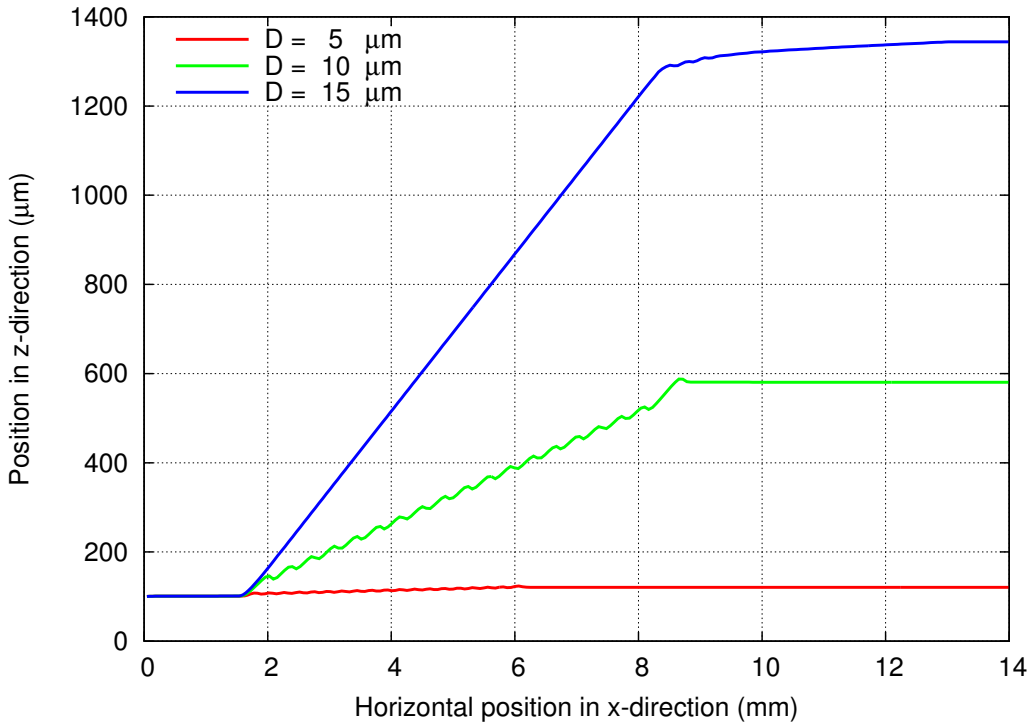

Figure 5.10: Deflection of three different particles with flow rate = 840 $\mu L/h$ and $V_{p-p} = 10\ V$

5.4.4 Channel height

Channel height is another design parameter that must be optimized to obtain an efficient separation process. As is depicted in Figure 5.11 by increasing the height of the channel, the effect of DEP force decreases. Therefore, for channel height of 60 μm the effect of DEP force is so low that the particle experiences no deflection. On the other hand, by decreasing the channel height to 20 μm the effect of DEP force becomes so high that the particle is deflected as it reaches the first electrode. In designing a microfluidic

device, channel height is of great importance. If it is lower than the optimal value and the particles are too large, clogging occurs in the channel and the separation process is almost impossible. If the height is larger than the optimal value, the effect of DEP force decreases and the particles are not deflected. In the current study, the channel height was chosen to be 40 μm.

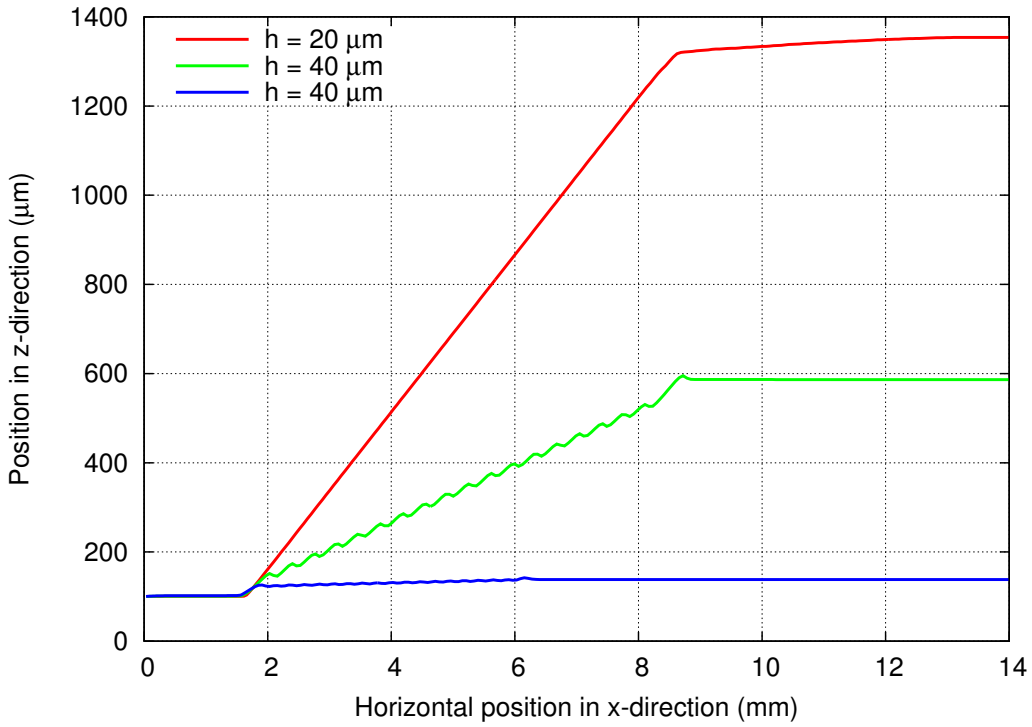

Figure 5.11: Effect of channel height on the trajectory of a 10 μm particle with flow rate=840 $\mu L/h$ and $V_{p-p} = 10\ V$

5.4.5 Number of electrodes

Figure 5.12 shows particle trajectory in channels with different number of electrodes. The number of electrodes plays an important role in how much the particles deflect. For instance, in a channel with five pairs of electrodes, an applied peak-to-peak voltage of $10V$and, a flow rate of 840 $\mu L/h$, the particle travels a total length of approximately 270 μm across the channel, while in a channel with higher number of electrodes, the particle travels a longer distance in the z-direction. Depending on the desired deflection, the

number of electrodes could change. Sometimes the applied voltage is so high that the particles are deflected as soon as they reach the first electrode. In this case, the number of electrodes is not required to be high. On the other hand, there are cases in which the voltage, the flow rate or the particle size is so low that the desired deflection is obtained only by increasing the number of electrodes. Figure 5.12 shows that there is a slightly high peak at the end of the electrode region. This peak is resulted from the fringing effect due to the non-uniformity of the electric field at the edge of the last electrode. This also occurs at the beginning edge of the first electrode.

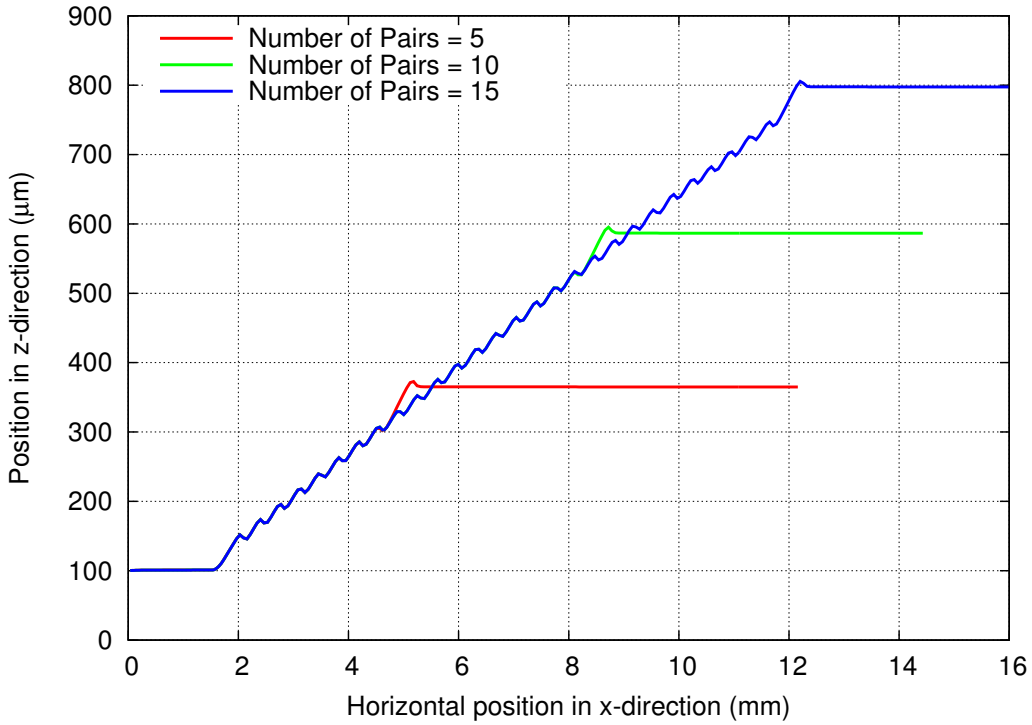

Figure 5.12: The effect of number of electrodes on the trajectory of a 10 μm particle with flow rate=840 $\mu L/h$ and $V_{p-p} = 10\ V$

5.5 Separation Process Modeling

Figure 5.13 is the top view of a cell separation process inside a microfluidic device for a case where 3000 particles with different sizes and properties were injected into the channel. This figure depicts the results obtained from the numerical simulation of the separation process in OpenFOAM. Yellow and green particles are target cells with diameters of 15 μm and 10 μm, respectively. Blue particles are non-target cells with a diameter of 10 μm. The particles were injected randomly through an inlet port on the left side of the channel with cross-sectional area of 40 μm $\times$ 200 μm. In this case, V_{p-p} is 10 V, and the flow rate is 840 $\mu L/h$. At the initial time of t=0.2 s, the particles are still in the entrance region and have not yet reached the electrode region. Note that at t=0.2 s, the blue and green particles are hidden by the large yellow particles and thus, are not visible to the eye. At t=0.6 s, the particles have entered the electrode region and there is a shift in their trajectory based on their sizes and properties. The yellow particles are the largest ones. Hence, the DEP force exerted on them is so strong that it is dominant over the drag force and the particles are deflected as soon as they reach the first electrode. As can be seen, the yellow particles move along the first electrode until they reach the region without electrodes. Then, they turn and travel in a straight path towards the first outlet. The green particles are smaller and the DEP force exerted on them is weaker compared to the yellow particles. Therefore, these particles enter the electrode region and become deflected by passing over each electrode. As soon as these particles leave the electrode region, they begin moving in a straight path towards the second outlet of the channel. Blue particles are the non-target cells that due to the lack of dielelectrophoretic properties, are not affected by the DEP force. These particles do not deflect at all and continue their straight path all the way towards the third outlet. As the time passes, the blue particles become more scattered since they do not possess dielectrophoretic properties, and thus, there is no DEP force pushing them towards the center of the channel. Additionally, the

only forces affecting the non-target cells are the drag force and the gravitational force. Therefore, the drag force reduces the speed of the non-target particles over the time and at the same time, the gravitational force pulls them towards the bottom of the channel. This may result in sedimentation of some of the non-target cells over the time which can be collected by flushing the microfluidic device. In addition to flushing the microfluidic device to collect the non-target particles, one could increase the flow rate during the separation process. However, increasing the flow rate requires an increase in the voltage to result in the same separation performance. As discussed earlier, the applied voltage is limited by the electrolysis of the medium and the viability of the cells.

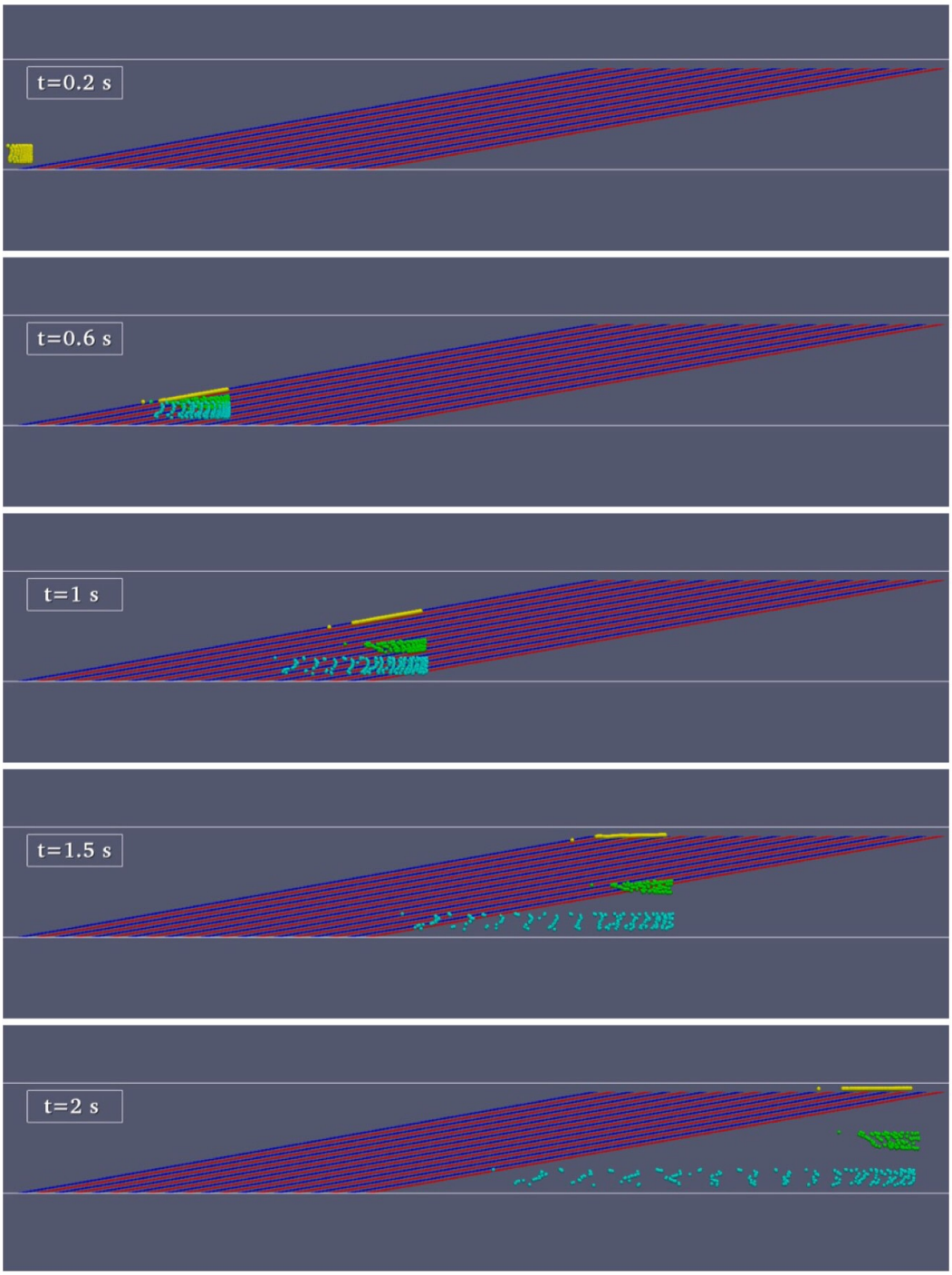

Figure 5.13: DEP separation process for two target cells with diameters of 15 μm and 10 μm (yellow and green), and one non-target cell with diameter of 10 μm (blue). $V_{p-p} = 10V$, flow rate=840 $\mu L/h$

CHAPTER 6

CONCLUSION

In this study, the deflection of the particles was successfully simulated in a dielectrophoretic bio-separation chip. The device consists of 10 pairs of slanted electrodes with an angle of 10° with respect to the direction of the flow. These electrodes are placed on the top and bottom walls of the channel and exert a repulsive force to the particles. Therefore, the net DEP force in the y-direction at the center of the channel is zero, and the deflection of the particles is mainly resulted from a combination of x and z components of DEP force as well as the hydrodynamic force. All simulations were performed using the open-source CFD software OpenFOAM and the deflection of the particles was predicted. A comprehensive parametric study was performed to investigate the effects of different parameters on the separation process. It was shown that by increasing the flow rate, the hydrodynamic force dominated the DEP force and the particles and less particle deflection occurred. The effect of voltage was also investigated. It was shown that by increasing the voltage, the DEP force increased and particles experienced a greater deflection. However, the electrolysis of the medium and the viability of the cells must be considered to determine a safe voltage level. Number of electrodes is another factor that influences the effectiveness of separation. As the number of electrodes increases, the deflection of the particles increases as well. This is due to the fact that increasing the number of electrodes, increases the time during which the particles are affected by the DEP force, which results in more deflection. In addition, it was shown that by decreasing the height of the channel, higher DEP forces can be generated at lower voltages. Therefore, for the same voltage and flow rate, particles in a channel with a height of 20 μm are deflected more than those in a channel with a height of 40 μm. However, it is important to note that decreasing the the channel height may cause a multitude of issues such as clogging of the channel and a reduced

throughput. One of most important parameters that was investigated was the effect of the the particle size. In fact, the primary purpose of dielectrophoretic microfluidic devices is to separate particles of different sizes. The DEP force has a cubic dependency on the radius of the particle. Therefore, for the same voltage and flow rate, the DEP force has a greater effect on larger particles and deflects them more than the smaller one. Thus, particles can be deflected and guided towards different collecting outlets and separated based on their sizes. Another parameter that was not investigated in this research due to lack of time, was the angle of electrodes. The main purpose of using slanted electrodes is to produce force in the z direction and to deflect the particles. By increasing the angle of the electrodes, the z-component of DEP force decreases and the particles tend to move in a straight path. When the electrodes are perpendicular to the direction of the flow, there is almost no force in the z-direction and the particles do not deflect at all. Finally, the results obtained from the simulation were compared to the results available in literature and found to be in good agreement.

REFERENCES

[1] H Pohl et al. The behavior of neutral matter in nonuniform electric fields. *Cambridge University Press, Cambridge*, 1978.

[2] Joel Voldman. Electrical forces for microscale cell manipulation. *Annu. Rev. Biomed. Eng.*, 8:425–454, 2006.

[3] Talukder Z Jubery and Prashanta Dutta. A new design for efficient dielectrophoretic separation of cells in a microdevice. *Electrophoresis*, 34(5):643–650, 2013.

[4] Andreas Lenshof and Thomas Laurell. Continuous separation of cells and particles in microfluidic systems. *Chemical Society Reviews*, 39(3):1203–1217, 2010.

[5] John Zelena. Electrokinetics of microparticles using ac dielectrophoresis, 2002.

[6] Yuejun Kang, Dongqing Li, Spyros A Kalams, and Josiane E Eid. Dc-dielectrophoretic separation of biological cells by size. *Biomedical microdevices*, 10(2):243–249, 2008.

[7] Soumya K Srivastava, Andreas Artemiou, and Adrienne R Minerick. Direct current insulator-based dielectrophoretic characterization of erythrocytes: Abo-rh human blood typing. *Electrophoresis*, 32(18):2530–2540, 2011.

[8] Talukder Z Jubery, Soumya K Srivastava, and Prashanta Dutta. Dielectrophoretic separation of bioparticles in microdevices: A review. *Electrophoresis*, 35(5):691–713, 2014.

[9] Stefan Fiedler, Stephen G Shirley, Thomas Schnelle, and Günter Fuhr. Dielectrophoretic sorting of particles and cells in a microsystem. *Analytical chemistry*, 70(9):1909–1915, 1998.

[10] Herbert A Pohl and Joe S Crane. Dielectrophoresis of cells. *Biophysical journal*, 11(9):711–727, 1971.

[11] Ronald Pethig and Gerard H Markx. Applications of dielectrophoresis in biotechnology. *Trends in biotechnology*, 15(10):426–432, 1997.

[12] Koichi Aoki. Theory of ultramicroelectrodes. *Electroanalysis*, 5(8):627–639, 1993.

[13] Xiaoyuan Hu, Paul H Bessette, Jiangrong Qian, Carl D Meinhart, Patrick S Daugherty, and Hyongsok T Soh. Marker-specific sorting of rare cells using dielectrophoresis. *Proceedings of the National Academy of Sciences of the United States of America*, 102(44):15757–15761, 2005.

[14] Robert G Ashcroft and Peter A Lopez. Commercial high speed machines open new opportunities in high throughput flow cytometry (htfc). *Journal of immunological methods*, 243(1):13–24, 2000.

[15] Jeffrey J Chalmers, Maciej Zborowski, Liping Sun, and Lee Moore. Flow through, immunomagnetic cell separation. *Biotechnology progress*, 14(1):141–148, 1998.

[16] Unyoung Kim, Chih-Wen Shu, Karen Y Dane, Patrick S Daugherty, Jean YJ Wang, and HT Soh. Selection of mammalian cells based on their cell-cycle phase using dielectrophoresis. *Proceedings of the National Academy of Sciences*, 104(52):20708–20712, 2007.

[17] Unyoung Kim, Jiangrong Qian, Sophia A Kenrick, Patrick S Daugherty, and H Tom Soh. Multitarget dielectrophoresis activated cell sorter. *Analytical chemistry*, 80(22):8656–8661, 2008.

[18] Swagatika Dash and Swati Mohanty. Dielectrophoretic separation of micron and submicron particles: a review. *Electrophoresis*, 35(18):2656–2672, 2014.

[19] R Diaz and S Payen. Biological cell separation using dielectrophoresis in a microfluidic device. *Bio and Thermal Engineering Laboratory–University of California B (ed). http://robotics. eecs. berkeley. edu/% 7Epister/245/project/DiazPayen. pdf*, 2008.

[20] Gerard H Markx, Ying Huang, Xiao-Feng Zhou, and Ronald Pethig. Dielectrophoretic characterization and separation of micro-organisms. *Microbiology*, 140(3):585–591, 1994.

[21] Il Doh and Young-Ho Cho. A continuous cell separation chip using hydrodynamic dielectrophoresis (dep) process. *Sensors and Actuators A: Physical*, 121(1):59–65, 2005.

[22] Hywel Morgan and Nicolas G Green. Dielectrophoretic manipulation of rod-shaped viral particles. *Journal of Electrostatics*, 42(3):279–293, 1997.

[23] Nai-Chin Chen, Chun-Hong Chen, Ming-Kun Chen, Ling-Sheng Jang, and Min-Haw Wang. Single-cell trapping and impedance measurement utilizing dielectrophoresis in a parallel-plate microfluidic device. *Sensors and Actuators B: Chemical*, 190:570–577, 2014.

[24] R Hamada, H Takayama, Y Shonishi, L Mao, M Nakano, and J Suehiro. A rapid bacteria detection technique utilizing impedance measurement combined with positive and negative dielectrophoresis. *Sensors and Actuators B: Chemical*, 181:439–445, 2013.

[25] Asuka Nakano, Tzu-Chiao Chao, Fernanda Camacho-Alanis, and Alexandra Ros. Immunoglobulin g and bovine serum albumin streaming dielectrophoresis in a microfluidic device. *Electrophoresis*, 32(17):2314–2322, 2011.

[26] Peter RC Gascoyne, Xiao-Bo Wang, Ying Huang, and Frederick F Becker. Dielectrophoretic separation of cancer cells from blood. *IEEE transactions on industry applications*, 33(3):670–678, 1997.

[27] Frederick F Becker, Xiao-Bo Wang, Ying Huang, Ronald Pethig, Jody Vykoukal, and PR Gascoyne. Separation of human breast cancer cells from blood by differential dielectric affinity. *Proceedings of the National Academy of Sciences*, 92(3):860–864, 1995.

[28] Anas Alazzam, Ion Stiharu, Rama Bhat, and Ari-Nareg Meguerditchian. Interdigitated comb-like electrodes for continuous separation of malignant cells from blood using dielectrophoresis. *Electrophoresis*, 32(11):1327–1336, 2011.

[29] Fang Yang, Xiaoming Yang, Hong Jiang, Phillip Bulkhaults, Patricia Wood, William Hrushesky, and Guiren Wang. Dielectrophoretic separation of colorectal cancer cells. *Biomicrofluidics*, 4(1):013204, 2010.

[30] Vishal Gupta, Insiya Jafferji, Miguel Garza, Vladislava O Melnikova, David K Hasegawa, Ronald Pethig, and Darren W Davis. Apostream, a new dielectrophoretic device for antibody independent isolation and recovery of viable cancer cells from blood. *Biomicrofluidics*, 6(2):024133, 2012.

[31] Mohammed Alshareef, Nicholas Metrakos, Eva Juarez Perez, Fadi Azer, Fang Yang, Xiaoming Yang, and Guiren Wang. Separation of tumor cells with dielectrophoresis-based microfluidic chip. *Biomicrofluidics*, 7(1):011803, 2013.

[32] Ronald Pethig, Ying Huang, Xiao-Bo Wang, and Julian PH Burt. Positive and negative dielectrophoretic collection of colloidal particles using interdigitated castellated microelectrodes. *Journal of Physics D: Applied Physics*, 25(5):881, 1992.

[33] Nicolas G Green and Hywel Morgan. Separation of submicrometre particles using a combination of dielectrophoretic and electrohydrodynamic forces. *Journal of Physics D: Applied Physics*, 31(7):L25, 1998.

[34] Nurul Amziah Md Yunus, Hossein Nili, and Nicolas G Green. Continuous separation of colloidal particles using dielectrophoresis. *Electrophoresis*, 34(7):969–978, 2013.

[35] Khashayar Khoshmanesh, Chen Zhang, Francisco J Tovar-Lopez, Saeid Nahavandi, Sara Baratchi, Arnan Mitchell, and Kourosh Kalantar-Zadeh. Dielectrophoretic-activated cell sorter based on curved microelectrodes. *Microfluidics and nanofluidics*, 9(2-3):411–426, 2010.

[36] Lisen Wang, Lisa A Flanagan, Noo Li Jeon, Edwin Monuki, and Abraham P Lee. Dielectrophoresis switching with vertical sidewall electrodes for microfluidic flow cytometry. *Lab on a Chip*, 7(9):1114–1120, 2007.

[37] Ali Hemmatifar, Mohammad Said Saidi, Arman Sadeghi, and Mahdi Sani. Continuous size-based focusing and bifurcating microparticle streams using a negative dielectrophoretic system. *Microfluidics and nanofluidics*, 14(1-2):265–276, 2013.

[38] J Voldman, M Toner, ML Gray, and MA Schmidt. Design and analysis of extruded quadrupolar dielectrophoretic traps. *Journal of electrostatics*, 57(1):69–90, 2003.

[39] Cheng-Hsin Chuang and Yao-Wei Huang. Multistep manipulations of poly (methylmethacrylate) submicron particles using dielectrophoresis. *Electrophoresis*, 34(22-23):3111–3118, 2013.

[40] Tai L Chow. *Introduction to electromagnetic theory: a modern perspective*. Jones & Bartlett Learning, 2006.

[41] Brian J Kirby. *Micro-and nanoscale fluid mechanics: transport in microfluidic devices*. Cambridge University Press, 2010.

[42] Matin Golozar, Majid Molki, and Jeff Darabi. Computational and performance analysis of a continuous magnetophoretic bioseparation chip with alternating magnetic fields. *Microfluidics and Nanofluidics*, 21(4):73, 2017.

[43] Majid Hejazian, Weihua Li, and Nam-Trung Nguyen. Lab on a chip for continuous-flow magnetic cell separation. *Lab on a Chip*, 15(4):959–970, 2015.

[44] Ronald Pethig. Dielectrophoresis: Status of the theory, technology, and applications. *Biomicrofluidics*, 4(2):022811, 2010.

[45] John Bird. *Basic engineering mathematics*. Routledge, 2017.

[46] EP Furlani. Analysis of particle transport in a magnetophoretic microsystem. *Journal of Applied Physics*, 99(2):024912, 2006.

[47] OpenFOAM. The open source computational fluid dynamics (cfd) toolbox. url-https://www.openfoam.com/.

[48] Shin-Hwung Lee. International journal of naval architecture and ocean engineering. *Journal DOI*, 2092:6790, 2015.

[49] J Santos and P de Oliveira. A converging finite volume scheme for hyperbolic conservation laws with source terms. *Journal of computational and applied mathematics*, 111(1):239–251, 1999.

[50] Joel H Ferziger and Milovan Peric. *Computational methods for fluid dynamics*. Springer Science & Business Media, 2012.

[51] Suhas Patankar. *Numerical heat transfer and fluid flow*. CRC press, 1980.

[52] OpenFOAM. Openfoam: Standard solvers. `https://www.openfoam.com/documentation/user-guide/standard-solvers.php`.

[53] Dimitri J Mavriplis. Mesh generation and adaptivity for complex geometries and flows. *Handbook of Computational Fluid Mechanics*, pages 417–459, 1996.

[54] Unyoung Kim and H Tom Soh. Simultaneous sorting of multiple bacterial targets using integrated dielectrophoretic–magnetic activated cell sorter. *Lab on a Chip*, 9(16):2313–2318, 2009.